Earth-Science Reviews 254 (2024) 104787

Contents lists available at ScienceDirect

Earth-Science Reviews

journal homepage: www.elsevier.com/locate/earscirev

Tectonic imprints in Permian paleomagnetic data of Morocco

Vinzenz Weissbrodt [a], Valerian Bachtadse [a], Uwe Kirscher [b,c,*], Hafid Saber [d], Yebo Liu [b], Ausonio Ronchi [e]

[a] Ludwig-Maximilians-Universität München, Department für Umwelt und Geowissenschaften, Sektion Geophysik, Theresienstrasse 41, 80333 Munich, Germany
[b] Earth Dynamics Research Group, The Institute for Geoscience Research (TIGeR), School of Earth and Planetary Sciences, Curtin University, Bentley, Western Australia 6102, Australia
[c] Eberhard Karls Universität Tübingen, Department of Geosciences, Sigwartstrasse 10, 72076 Tübingen, Germany
[d] Chouaïb Doukkali University, Faculty of Sciences, Department of Geology, Laboratory of Geodynamic and Geomatic, B.P. 20, 24000 El Jadida, Morocco
[e] Università di Pavia, Dipartimento di Scienze della Terra e dell'Ambiente, Via Ferrata 1, 27100 Pavia, Italy

ARTICLE INFO

Keywords:
Pangea
Supercontinent assembly
Paleogeography
Paleomagnetism

ABSTRACT

Although Pangea as Earth's youngest supercontinent has continuously served as a pivotal reference mark in paleogeographic reconstructions, its assembly is still a matter of debate. This is mainly due to poor paleomagnetic data coverage for Permian times for Africa, core element of Pangea. Paleomagnetic data from Adria, thought to be the African promontory in the Permian, yield paleolatitudes which, when compared to the European data set, result in a significant continental overlap and seem to confirm the original Pangea B concept of Irving (1977). In order to improve the paleomagnetic data situation for Africa, volcanic and sedimentary rocks were sampled in the Permo-Carboniferous basins of Morocco, yielding a total of 97 sites and 615 samples. Rock magnetic results are diagnostic for magnetite and hematite in various proportions as main carriers of the paleomagnetic signal. After removal of low and intermediate coercivity/blocking temperature components a characteristic component of magnetization pointing to the SE with declinations strung out along a small circle from 107° to 182° and with inclinations around −7° after tectonic correction was identified in 76% of the samples. In nine out of the ten basins studied, positive inclination only fold tests support the primary character of magnetization. Furthermore, three reversals were identified at the basins of M'Tal, Chougrane and Souk El Had Bouhsoussene lending further support to our interpretation of primary magnetization. VGPs are distributed along a NE-SW trending small circle band intersecting the Late Paleozoic segment of the Gondwana APWP with a rotation pole located in the sampling area. The resulting paleolatitudes yield a position of the Meseta block close to the paleo-equator at ~280 Ma. The widespread presence of vertical axis rotations in the Meseta basins on the other hand, could be related to proposed intra-Pangea shear zones and would provide additional constraints on the extent of such shear zones towards the northern margin of Gondwana. However, tectonic models based on vertical axis rotations in this region need to be treated with caution, since the timing of these rotations remains ambiguous with the current data situation. Using our paleomagnetic data from the Meseta block as representative for Gondwana, a large latitudinal overlap between Gondwana and Laurussia is not required.

1. Introduction

Since the identification of Pangea, the importance of supercontinents for the geosphere and biosphere in Earth evolution gained increasing attention (Mitchell et al., 2021). As the most recent and therefore likely to be the best understood supercontinent, Pangea plays a key role as reference point in plate tectonic modelling for post-Paleozoic times. However, its geometry and geodynamic evolution are continuously debated and details of its paleogeography for Late Paleozoic times are not yet completely agreed on (Channell et al., 2022; Pastor-Galán, 2022; Wu et al., 2021). While Pangea's break-up process from Jurassic times onward has mostly been deciphered using the large paleomagnetic data set and seafloor data, its paleogeographic evolution remains ambiguous for prior times (e.g., Aubele et al., 2012; Edel et al., 2018; Muttoni et al., 2003; Pohl et al., 2018). High quality data for the Late Paleozoic – especially from Gondwana – is still scarce leading to substantial

* Corresponding author at: Earth Dynamics Research Group, The Institute for Geoscience Research (TIGeR), School of Earth and Planetary Sciences, Curtin University, Bentley, Western Australia 6102, Australia.
E-mail address: uwe.kirscher@curtin.edu.au (U. Kirscher).

https://doi.org/10.1016/j.earscirev.2024.104787
Received 13 August 2023; Received in revised form 18 April 2024; Accepted 21 April 2024
Available online 26 April 2024

uncertainties in paleogeographic reconstructions. These uncertainties led some authors to argue for a substantial latitudinal overlap of Laurasia and Gondwana when keeping the general continental assemblage in a conventional Wegenerian or Pangea A configuration for the early Permian (Muttoni et al., 2009; Muttoni et al., 2003). To avoid this misfit Irving (1977) as well as Morel and Irving (1981) introduced an alternative configuration labelled Pangea B. Here, Gondwana is shifted approximately 3000 km to the East with respect to the northern continents (Laurasia) along a constant line of latitude. In order to accomplish the transition of the assumed Pangea B model to the widely approved Pangea A model an early Permian diffuse dextral shear zone was introduced which was located in the Mediterranean and has been related to structural vertical axis rotations of pre-late Permian tectonic blocks (Aubele et al., 2014; Aubele et al., 2012; Bachtadse et al., 2018; Kent and Muttoni, 2020; Muttoni and Kent, 2019) (see next chapter for more details on the Pangea controversy).

Since conclusive evidence is still lacking, a variety of explanations for the validity of Pangea B have been controversially discussed (see review and references in Domeier et al. (2012)). Among them, complementing the sparse Permian paleomagnetic information of Gondwana with data from Adria, i.e. treating Adria as a tectonically coherent African promontory, has on one hand turned out to be one of the main arguments for the presence of the latitudinal misfit, but on the other hand has been criticized in lacking legitimacy (a comprehensive historical background is provided by Muttoni and Kent (2019)). Domeier et al. (2021) tackled this issue by highlighting relative motions between Adria and Africa due to the opening of the Ionian basin and criticized biasing effects on African paleolatitudes towards higher values (thus favouring Pangea B) when utilizing the relatively high amount of data from Adria as a proxy for Gondwana. Furthermore, their early Permian paleogeographic reconstruction based on Moroccan (i.e. NW African) volcanics showed no latitudinal misfit. In response, Channell et al. (2022) propose a kinematic model that reconciliates Mediterranean tectonism with its effect on paleomagnetic data from Adria shifting Africa towards the north. They further indicate that, due to general paucity of available data, the validity of Pangea A or Pangea B critically hinges on selection and filtering criteria. Domeier et al. (2012) suppose that especially inclination-shallowing prone sediments from the scarce Gondwanan data set might be responsible for the overlap and that applying a blanket flattening correction factor f of 0.6 (Tauxe, 2005) largely resolves the latitudinal misfit. However, this leads to significant increase in scatter of the sedimentary data set and reduces the consistency with data from coeval volcanic rocks (Channell et al., 2022). Hence, obtaining additional high-quality early Permian data from Gondwana becomes indispensable for a substantial progress in the Pangea debate and reconstruction of Late Paleozoic paleogeography.

In this context, the Moroccan Meseta (MM) in NW-Africa fits the requirements to play a key role for unravelling the paleogeographic position of the northern margin of Gondwana – and because the relationship of the MM and Africa is much better constrained and minor in its extend compared to the Adria-Africa relationship, also for Gondwana itself – during the late Carboniferous and early Permian to complement the poor Late Paleozoic data set. After publication of the pioneer studies of Daly and Pozzi (1976), Martin et al. (1978) and Westphal et al. (1979), it took more than four decades until Domeier et al. (2021) presented new paleomagnetic as well as geochronologic data providing additional information to determine the early Permian position of Gondwana. They presented a comparably low number of sites (20) from six basins and found some conspicuous features within their results, such as *syn*-folding or inconclusive (inclination-only) foldtests or NE-SW elongate girdling of the VGPs. The authors explain the syn-folding maximum clustering with either a primary magnetization that was affected by minor tectonic complexities or an actual remagnetized signal related to the terminal phase of the Variscan orogeny at ~275 Ma, which caused the minor tilting in this region. Potential influence of vertical axis rotations is interpreted to have been partially averaged out in the overall magnetic direction but ultimately the authors cannot provide an unambiguous interpretation due to their small data set (Domeier et al., 2021).

In this study we present a review of published paleomagnetic results for the Moroccan Meseta block incorporating results of newly collected 615 samples from 97 sites in ten basins. A combination of red sediments and intercalated volcanic flows allows the identification of tectonic attitudes of the volcanic rocks as well as direct testing of inclination shallowing in the sediments. We base the new results on the most recent age estimates using radiometric dating, paleontology and stratigraphy (Domeier et al., 2021) and georeferenced our samples in order to correlate them with given geological and geochronological constraints (Figs. S1-S9, Tables S1-S10).

2. The Pangea debate

Since the landmark papers of Irving and Morel (1978), Morel and Irving (1981) and Morel et al. (1981) in the late seventies and early eighties, a vivid debate has been triggered, which is still ongoing (Channell et al., 2022; Domeier et al., 2021; Irving, 2013; Kent and Muttoni, 2020; Muttoni et al., 2013; Muttoni et al., 2003). Irving (1977) recognized that reconstructing a Permian Pangea in a Wegenerian (Pangea A) constellation and using paleomagnetic data to determine the paleolatitudes of Laurentia's southern and Gondwana's northern margins, resulted in a significant overlap of both continents. This overlap can be resolved by shifting Gondwana some 3000 km to the east, thus positioning northwest Africa directly opposite the Donetsk basin (Morel et al., 1981), but simultaneously maintaining its paleolatitude. Since paleolongitudes are undefined using conventional paleomagnetic data, this approach would not violate any principle of paleomagnetic reconstructions. The resulting reconstruction (Pangea B), however, created new problems.

There is no doubt that the opening of the Atlantic Ocean started from within a Pangea A configuration, thus requiring a mega shear zone, along which, Gondwana moved some 3000 km to the west sometimes between the early Permian and the Early Jurassic. The formation of Permian rift basins such as the Oslo-Polish and the eastern Mediterranean basins as well as the intramontane basins in central Europe, Greenland, northern Africa and northeastern America can be linked to a right lateral shear zone connecting Urals and Appalachians as originally proposed by Van Hilten (1964) and subsequently revived by Arthaud and Matte (1977). However, despite the evidence for oblique collision between Gondwana and North America (Becker et al., 2005) the existence of this mega shear zone, the main prerequisite for any Pangea B type configuration is still controversial. Regardless of the paleomagnetic arguments (Muttoni et al., 2003; Torcq et al., 1997) and additional paleoclimatological (Fluteau et al., 2001), paleontological (Silantiev et al., 2022; Vai, 2003) as well as geochemical (Becker et al., 2005) evidence for the realistic possibility of Pangea B configurations, the strongest opposition arises from within the paleomagnetic community itself. Main arguments being that the continental misfit between Laurentia and Gondwana is an artifact caused by (a) long living quadru- and octupole elements of the Earth's magnetic field (Van der Voo and Torsvik, 2001), (b) incorrect dating and/or correlating Permian rocks from both continents (Rochette and Vandamme, 2001) or (c) inclination shallowing (Domeier et al., 2012), a process affecting the orientation of magnetic minerals during compaction (King, 1955) of sediments not uncommon in continental red beds (Kirscher et al., 2014; Tauxe and Badgley, 1984), which form a significant part of the Permian paleomagnetic database for Gondwana and Laurentia. Whereas at least (a) has been discounted recently (Domeier et al., 2012; Evans et al., 2014), (b) and (c) are still options, whereby (c) is currently preferred by the majority of the paleomagnetic community. Based on this rationale Domeier et al. (2012) published a set of apparent polar wanders paths (APWP) and paleogeographic reconstructions for Gondwana and Laurentia. Accounting for inclination shallowing Domeier et al. (2012) applied a

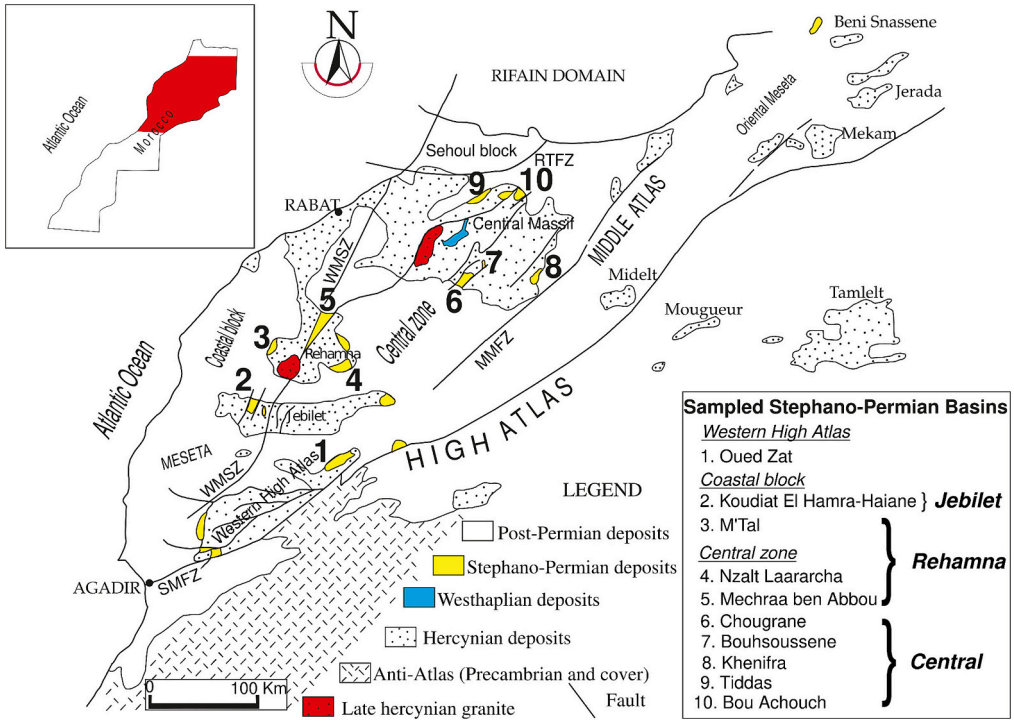

Fig. 1. Schematic structural and geological map of the sampling area in the Moroccan Variscides. Delimitation of main tectonomorphic domains after Chopin et al. (2014), Hoepffner et al. (2005), Hoepffner et al. (2006), Michard et al. (2008), Michard et al. (2010a), Michard et al. (2010b). WMSZ: Western Meseta Shear Zone, RTFZ: Rabat-Tiflet Fault Zone, MMFZ: Middle Meseta Fault Zone, SMFZ: South Meseta Fault Zone. Stephanian and Westphalian are regional Western European stages of the late Carboniferous (Gradstein et al., 2020) used due to the biostratigraphic constraints of ZAT.

blanket flattening factor (Tauxe and Kent, 2004) of f = 0.6 on all paleomagnetic data based on sedimentary rocks, irrespectively whether these rocks were of marine or continental origin, clastic or chemical sediments and thereby eliminating the continental overlap. Whether the application of a blanket correction for inclination shallowing is correct, remains a matter of debate. Especially questionable is the basic assumption made by Domeier et al. (2012) that all sediments suffer the same amount of flattening. In fact it has been demonstrated that inclination shallowing in sedimentary rocks of various ages and different lithologies can actually range from no shallowing at all (f = 1.0) to rather severe shallowing (f = 0.4) where no systematic correlation between rock type and degree of shallowing is observable (Kodama, 2012, pages 54 and 62). It is also noteworthy that Muttoni et al. (2013), by limiting their data selection to volcanic rocks of early Permian age from Africa and the southern Alps and thereby circumventing the problem of inclination shallowing could show that the continental misfit might be real and therefore argue in favour of Pangea B models.

Recently published paleomagnetic results for Permian rocks of Sardinia and the Provence (Aubele et al., 2014; Aubele et al., 2012; Bachtadse et al., 2018) agree with the existence of an intra-Pangean shear zone which is characterized by complex and differential clockwise as well as counterclockwise block rotations that may have largely occurred during the early Permian, certainly prior to the Jurassic (Kirscher et al., 2011). These rotations have tentatively been assigned to represent shear stresses caused by a large intra-Pangean dextral transform fault system which is required to transfer Gondwana from a Pangea B into a Pangea A configuration compatible with the Arthaud and Matte (1977) concept but also with a geodynamic interpretation of shear systems within Gondwana (see Fig. 4 in Visser and Praekelt, 1998). Despite that these rotations are compatible with interpretations of the region as a diffuse plate boundary (sensu Gordon, 1998) caution should be used when interpreting these as the"smoking gun" supporting the validity of Pangea B.

3. Geologic setting, sampling and geochronological constraints

The Late Paleozoic collision of Laurussia and Gondwana with associated terranes created the Hercynian belt extending ~8000 km from the Appalachians to the Urals forming the supercontinent of Pangea. The complex geometry of the colliding continents (Guiraud et al., 2005) as well as a time-variable stress pattern (e.g. Chopin et al., 2014; Wernert et al., 2016) defined both a transpressional and transtensional tectonic framework combined with an intracontinental strike-slip shear network (Elter et al., 2020; Hoepffner et al., 2006). The Mauritanide segment of the Variscan orogeny in North Africa is predominantly exposed in Morocco and forms the Moroccan Variscides at the NW margin of Gondwana (Hmich et al., 2006; Michard et al., 2010b). The Mauritanides can be interpreted as the southwestern prolongation of its European counterpart (Chopin et al., 2014; Elter et al., 2020; Hoepffner et al., 2006; Hoepffner et al., 2005; Michard et al., 2010a; Michard et al., 2008; Michard et al., 2010b; Wernert et al., 2016; Zouicha et al., 2022).

Among the Moroccan Variscides, Pennsylvanian-Permian successions are documented mainly in the Western High Atlas and the Western Moroccan Meseta, an area which is roughly confined by a set of dextral wrench faults: the Rabat-Tiflet Fault Zone (RTFZ) to the north, the Middle Meseta Fault Zone (MMFZ) to the east and the South Meseta Fault Zone (SMFZ) to the south (Fig. 1; Chopin et al., 2014; Hoepffner et al., 2005; Michard et al., 2010a; Wernert et al., 2016).

The Western High Atlas of Morocco (WHA) displays a NE-SW elongated morphology subparallel to the Paleozoic Anti-Atlas mountain range divided by the SMFZ. In contrast to the prevalent Mesozoic layers of the Central High Atlas, the WHA mostly consists of Paleozoic and Precambrian deposits (Fig. 1). Since the WHA has been shaped by a variety of tectonic deformation processes, i.e. the initial compressional stage of the Variscan orogeny along dextral wrenching by the SMFZ, Permian-Jurassic continental rifting, Early Cretaceous inversion and mid-Jurassic to Early Cretaceous uplift as well as ultimate Late Cretaceous-Cenozoic shortening, it can be regarded both an oblique slip-

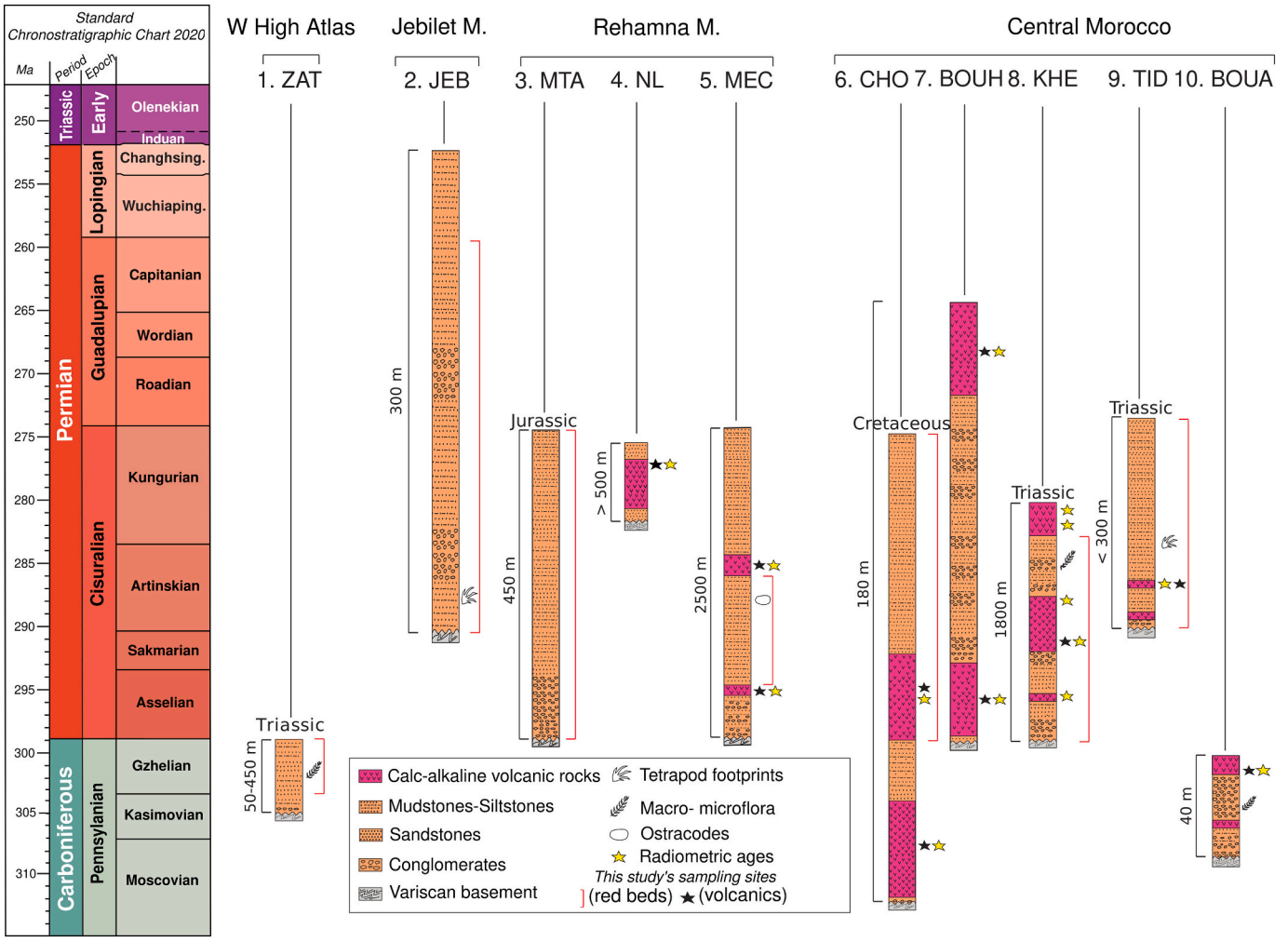

Fig. 2. Lithostratigraphic correlation of sampled late Carboniferous-Permian basins in Morocco with sampling horizons together with paleontological and radiometric age constraints (see text for further information and references) ordered by corresponding Late Paleozoic domains from south to north (numbering as in Fig. 1). Standard Chronostratigraphic chart after Gradstein et al. (2020). Basin abbreviations as in Table 1.

structure and an intracontinental fold-and-thrust belt (e.g. Barbero et al., 2011; Lanari et al., 2020; Perez et al., 2019; Skikra et al., 2021 and references therein).

The Western Meseta (WM) is a tabular domain crossed by the dextral Western Meseta Shear Zone (WMSZ) separating the coastal block to the west from the central zone to the east. Accordingly, Paleozoic massifs of the WM (i.e. Jebilet, Rehamna and Central Massif) are split by the WMSZ into segments belonging to the coastal block (Western Jebilet and Western Rehamna) and the central zone (Eastern Jebilet, Eastern Rehamna and the Central Massif) (Fig. 1; Barbero et al., 2011; Chopin et al., 2014; Delchini et al., 2016; Essaifi and Hibti, 2008; Hoepffner et al., 2006; Hoepffner et al., 2005; Michard et al., 2008; Michard et al., 2010b; Saddiqi et al., 2009).

During the transition from the Upper Carboniferous to the lower Permian, principal compressional stress axes changed from N-S to E-W in the WHA and WM which initiated the final phase of the overthickened Variscan orogenic belt (e.g. Doblas et al., 1998; Hadimi et al., 2021; Michard et al., 2008). Gravitational collapse and simple pure shear low-angle extensional detachments induced by the system of dextral strike-slip faults introduced a transtensional tectonic framework forming a Basin-and-Range-type province. As a consequence, synextensional plutonic bodies were emplaced, metamorphic core domains were unroofed and enhanced calc-alkaline magmatic activity created various volcanic deposits as well as dike/sill swarms. Moreover, continental pull-apart basins were contemporaneously formed during the Stephanian-Autunian (Fig. 1; Chopin et al., 2014; Doblas et al., 1998; Hadimi et al., 2021; Hoepffner et al., 2006; Michard et al., 2008). These isolated transtensional, rhomb-(half)graben-like or domino-like intramontane basins are preferably oriented N(*N*)E-S(*S*)W parallel to the predominant dextral fault system and are filled with continental sedimentary deposits (e.g. terrestrial red beds and siliciclastic molasses) with potential intercalations of bimodal volcanic lava flows (mainly of basaltic to trachy-andesitic and dacitic to rhyolitic affinity), pyroclastic episodes and assemblages of dikes and sills (Barbero et al., 2011; El Hadi et al., 2014; El Wartiti et al., 1990; Elter et al., 2020; Hadimi et al., 2021; Hoepffner et al., 2006; Michard et al., 2008; Voigt et al., 2011b; Zouicha et al., 2022).

Those pull-apart basins were all created within a setting of major intracontinental strike-slip shear motion (Elter et al., 2020). This broad-scale shear network might act as a geological cornerstone for the mobility between Laurasia and Gondwana and thus for the validity of the Pangea 'B' model. In such a transform fault system, bigger geologic domains are expected to undergo block rotation in ball bearing type setting which can be quantified by variations of the paleomagnetic declination (Aubele et al., 2014; Aubele et al., 2012). Thus, it may be hypothesized that samples from basins close to the boundary of the continental-scale shear zone (i. e. in the north of Morocco) might be significantly more affected by vertical axis rotations than more distant basins (i.e. to the south).

Ten Late Paleozoic basins were studied (Figs. S1-S9, Tables S1-S10).

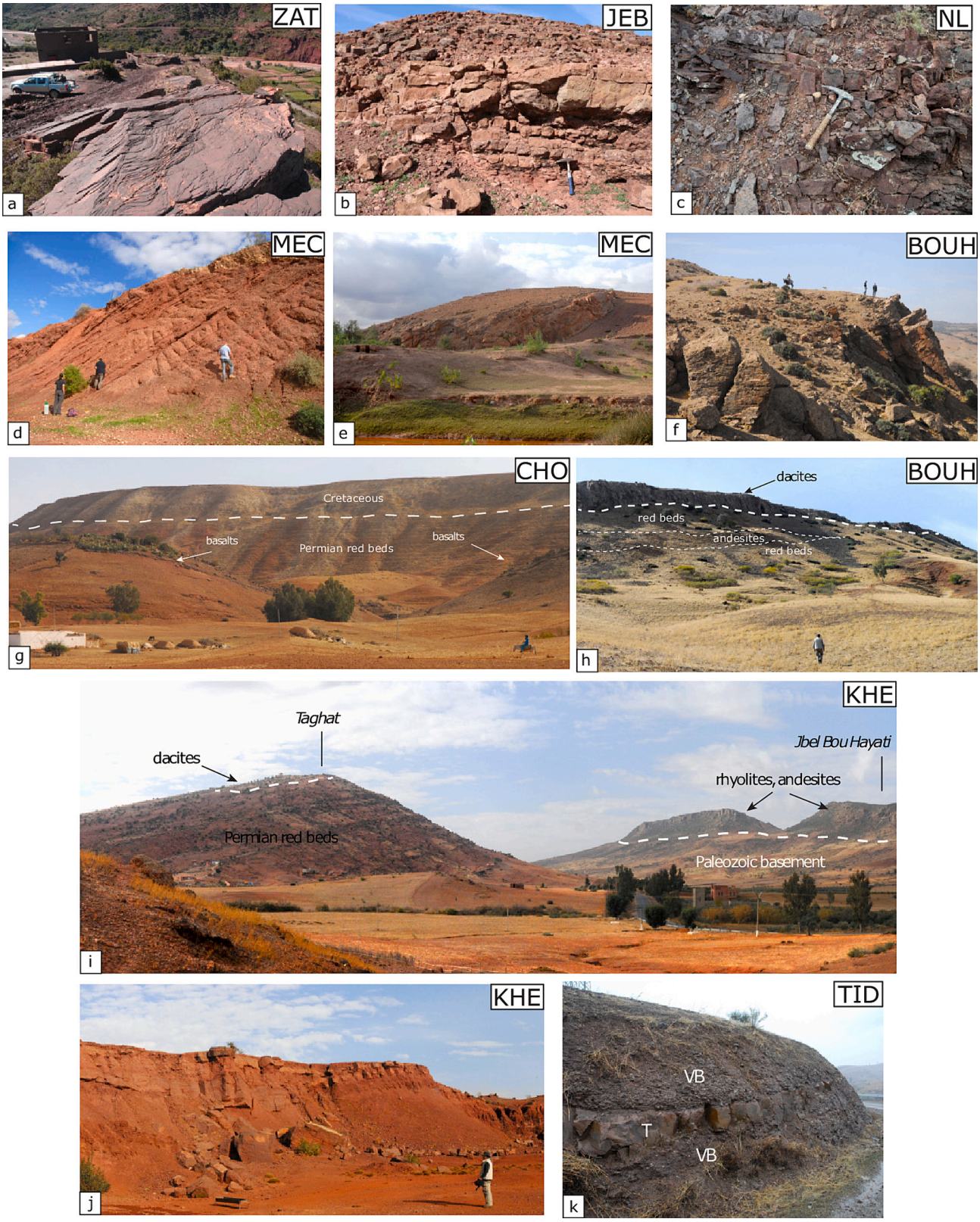

Fig. 3. Field observations from selected sampled Late Paleozoic basins in the Western High Atlas and Western Meseta of Morocco. a) late Carboniferous fine-grained violet deposits in the Oued Zat basin. b) Panoramic view of the Koudiat El Hamra-Haiane basin profile (Jebilet Massif). c) Close-up of the andesite lava flows in the Nzalt-Lararcha basin (Rehamna Massif). d) Medium-coarse debris flow deposits in the Mechraa ben Abbou basin (Rehamna Massif). e) Bled Mekrach garnet-bearing rhyolitic dome in the MEC basin profile. f) Dacites/andesites at the top of El Had Bouhsoussene basin profile. g) Panoramic view of the volcano-sedimentary succession of Chougrane basin. h) Panoramic view of the volcano-sedimentary succession of BOUH. i) Panoramic view of Khenifra basin from E to W. j) Coarse- to medium-grained red beds in KHE basin (El Messalla quarry). k) Tuff layers (T) intercalated with volcanic breccias (VB) in the Tiddas basin (Ait Ikkou locality). (For interpretation of the references to colour in this figure legend, the reader is referred to the web version of this article.)

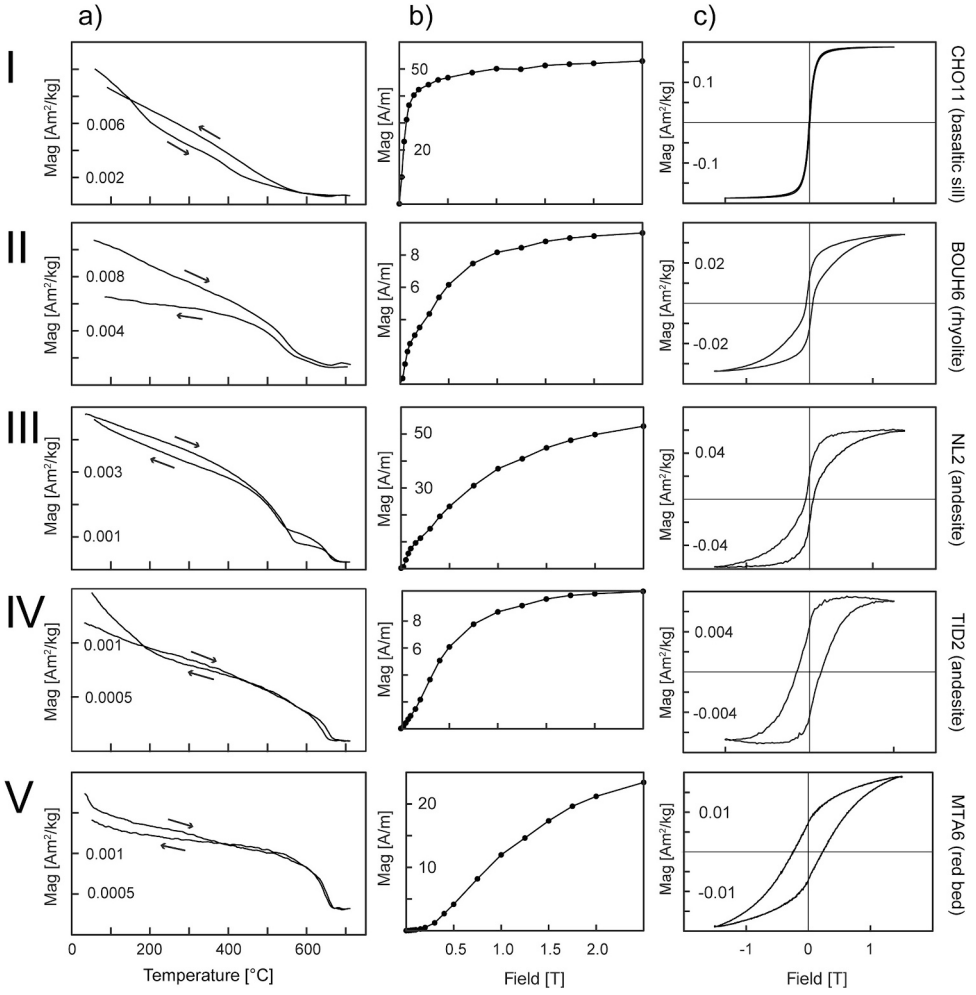

Fig. 4. Representative rock magnetic results subdivided according to lithology, where groups I-IV were derived from volcanic samples of various affinities and group V represents sedimentary, predominantly red bed samples. For each category, thermomagnetic curves (a), IRM-curves (b) and hysteresis-loops (c) are provided. Arrows specify heating and cooling cycles of thermomagnetic curves.

These are Oued Zat (ZAT) from the WHA, Koudiat El Hamra-Haiane from the Jebilet massif (JEB), M'Tal (MTA), Nzalt-Lararcha (NL) and Mechraa Ben Abbou (MEC) from the Rehamna Massif and ultimately Chougrane (CHO), El Had Bouhssoussene (BOUH), Khenifra (KHE), Tiddas-Souk Es-Sebt des Ait Ikko (Tsesdai) – in short Tiddas (TID) and Bou Achouch (BOUA) from the Central Massif where we extracted a total of 615 samples from 97 sites for rockmagnetic and paleomagnetic analysis (Fig. 1).

Hereafter we briefly summarize the geological, stratigraphic, paleontological and geochronological setting of each individual basin and comment on a possible age model of our samples using available age constraints (Fig. 2). Whenever there was comparable data available from literature for the studied basins, we included them in the age model in order to enlarge the data set.

3.1. Oued Zat (ZAT)

In ZAT rocks crop out in the northern prolongation of the WHA (Figs. 1, S1) on the road between Ouarzazate and Tighadwiyn. Its late Carboniferous basin fill is marked by increasing thickness towards the south ranging from 50 to 450 m, is unconformably capped by Triassic red beds and is composed of the following sedimentary formations from base to top: 1) the basal Tighadwiyn Formation is composed of purplish red conglomerates with rounded quarzite pebbles. The base is erosive and rests unconformably over the green-yellowish flysch of the Visean basement; 2) the upper Mçtour Formation is composed of grey-purple to grey-brownish quartz-rich very fine sandstones (Fig. 3a), clays and silts containing greenish grey levels with carbonaceous lenses, native sulphur and remains of Stephanian B—C flora (Fig. 2; Doubinger and Roy-Dias, 1985; Saber and El Wartiti, 1996; Saber et al., 2007).

Therefore, the Mçtour Formation can be roughly attributed to the Gzhelian (303.68 Ma – 298.90 Ma, Aretz et al. (2020)). From this upper part, 74 samples have been drilled at twelve sites (Fig. S1, Table S1).

3.2. Koudiat El Hamra-Haiane (JEB)

The Koudiat El Hamra- Haiane basin is located in the western Jebilet Massif (Figs. 1, S2). Its stratigraphic succession shows about 300 m thick siliciclastic deposits with alternation of grey brownish shaly-silty to sandy horizons in the lower part and reddish sandstones to quartz-rich microconglomerates in repeated fining-upward sequences in the middle–upper portion (Fig. 3b). Red-ocher calcretes are very frequent in the lower–middle part of the profile (Zouicha et al., 2022). Again, the middle–upper part of the section shows strongly oxidized dark-red coarse sandstones, which contain many plant fragments and roots that suggest wet conditions (Fig. 2; Huvelin, 1977).

The formation of the Koudiat El Hamra-Haiane basin has initially been attributed to the Westphalo-Permian by Huvelin (1977) which was also confirmed by Delchini et al. (2018). Recently, a first record of invertebrate and vertebrate trace fossils was reported by Zouicha et al.

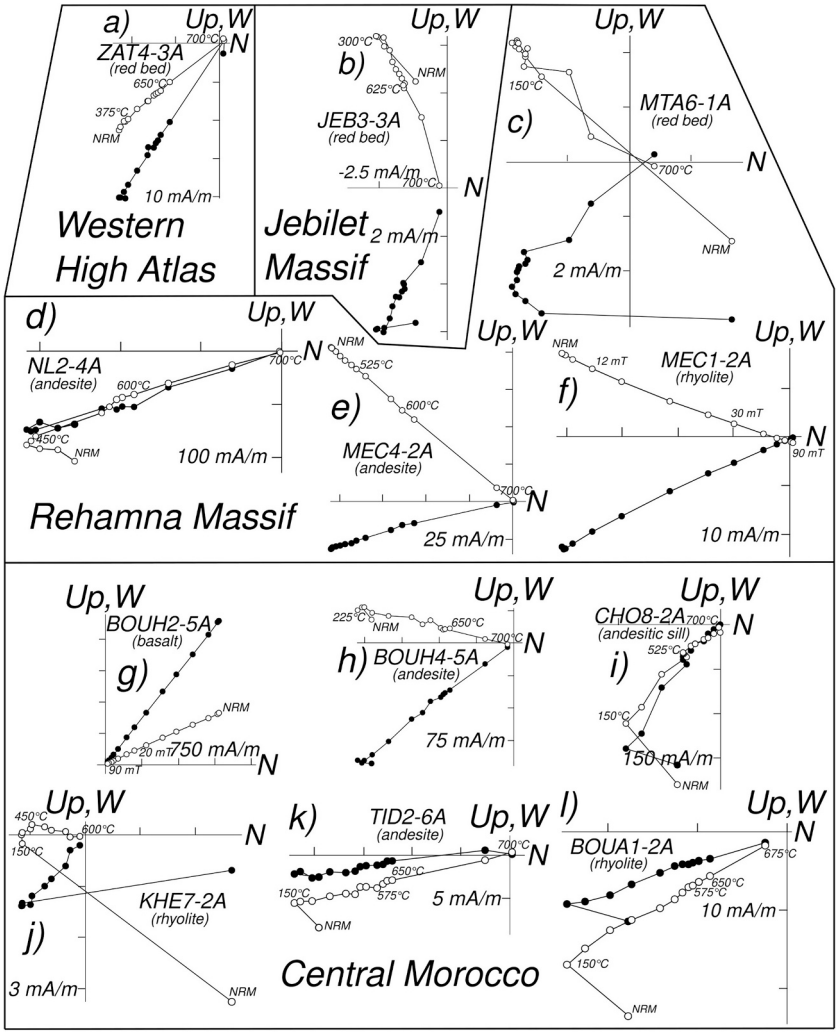

Fig. 5. Paleomagnetic results of demagnetization experiments of representative samples plotted as orthogonal vector diagrams after Zijderveld (1967) in geographic (in situ) coordinates. Solid (open) dots describe the vector endpoints projected onto the horizontal (vertical) plane and some of them are labelled with their respective demagnetization steps (in [mT] for AF demagnetization and in [°C] for thermal demagnetization) or the NRM.

(2021) in the lower beds of Koudiat El Hamra – Haiane sections suggesting a late early Permian (Artinskian) to middle Permian (Capitanian) age, i.e. 290.51–259.55 Ma following Henderson et al. (2020).

In the Koudiat El Hamra-Haiane basin we obtained 31 samples at five red bed sites (Fig. S2; JEB3- JEB8; due to their almost identical position and low number of samples taken at the last site we treat JEB7 and JEB8 as one site JEB7_8). Since one core's orientation could not be retrieved, 30 red bed cores have been paleomagnetically measured (Table S2).

3.3. M'Tal (MTA)

The M'Tal basin, westernmost part of the Rehamna Massif, crops out approximately 100 km south of El Jadida, on the road to Marrakech near Jemaâ M'tal (Figs. 1, S3). According to Saber et al. (2014), the approximately 450 m thick reddish succession consists of a lower part dominated by conglomerates with abundant matrix (Ouled Mira formation) overlain by a succession of sand-siltstones (Bir Enhass formation) (Fig. 2).

A systematic analysis of the synsedimentary fracturing reveals that the fault network and the opening of the MTA basin was activated during East-West extension. Based on the analogy of the facies, the geological history and the geographical proximity, the deposits of MTA basin are considered as related to those in the MEC basin, which are Cisuralian (Damotte et al., 1993; Saber et al., 2014), i.e. 298.89–274.37 Ma in age (Henderson et al., 2020). From these early Permian red beds of MTA, we drilled 41 cores at seven sites (Table S3).

3.4. Nzalt-Larancha (NL)

NL is located in the south-eastern part of the Rehamna Massif (Figs. 1, S4). The volcano-sedimentary succession is represented by the Sidi Yahia formation exceeding 500 m (Saidi et al., 2002) and is unconformably deposited over the Hercynian basement (Michard, 1976; Michard, 1982). Corresponding sediments, consisting of fine-to-coarse-grained clastics, bracket a series of volcanics (Fig. 3c; Charif et al., 1998). Recent dating from a rhyolite in this basin (Sidi Bou Yahia dome) provided a $^{206}Pb/^{238}U$ weighted mean age of 277.07 ± 0.61 Ma, which represents the first absolute age constraint from this basin (Fig. 2; Domeier et al., 2021).

In the NL basin, we extracted 71 cores of mainly andesitic affinity at eleven different sites (Fig. S4, Table S4). Since we observed the geochronologically dated dome of Sidi Bou Yahia to interfinger with our adjacent, sampled andesites, a mean age of 277.07 ± 0.61 Ma has been assumed for all samples taken at NL (Table S4).

3.5. Mechraa Ben Abbou (MEC)

The basin of MEC is part of the northern Rehamna Massif and is

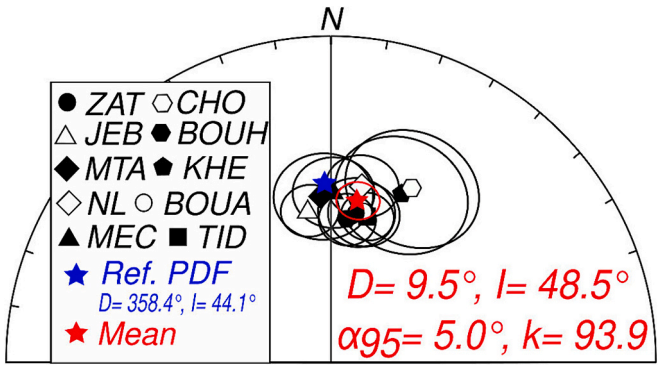

Fig. 6. Stereographic projection of the individual basins' low temperature paleomagnetic mean directions (black symbols associated with respective basins are given in the inset) in geographic (in situ) coordinates surrounded by their corresponding α_{95} confidence intervals (black circles). The referential present-day field (PDF) for the sampling area in Morocco is visualized by a blue star and given in the inset, as well. The overall mean direction of all basins is marked by a red star and related quantities like mean declination, mean inclination as well as Fisher (1953) parameters (α_{95} and k) are given within the stereoplot. α_{95} is the fisher angle of half cone of 95% confidence around the mean direction and k is the fisher precision parameter of the mean direction. (For interpretation of the references to colour in this figure legend, the reader is referred to the web version of this article.)

predominantly filled by clastic deposits (Figs. 1, S5; Damotte et al., 1993; El Kamel, 1987; El Wartiti et al., 1992; El Wartiti et al., 1990). The huge fining-to-coarsening upward red-bed succession with an estimated thickness of about 2500 m is interrupted by two volcanic pulses and can be subdivided into two sequences. The lower segment starts with talus-cone conglomerates-breccias, evolving into fluvial sandstones and floodplain deposits. Then the sequence continues in the middle-upper part again with thick fluvial deposits and mudflows (Fig. 3d). In the fine-grained middle part of the succession, rare lacustrine carbonates and mudstones contain stromatolites, algal buildings and an ostracod fauna, which permit to ascribe the series to the Cisuralian (Fig. 2; Damotte et al., 1993), i.e. 298.89–274.37 Ma (Henderson et al., 2020).

The volcanic rocks of MEC are intercalated in the red beds (e.g. Gigout, 1951; Hoepffner, 1982) and appear as massive/fluidal andesitic lava flows, interspaced to the lower clastic deposits of the first sedimentary sequence, and as rhyolitic domes associated with the second sequence (e.g. the Bled Mekrach garnet-bearing rhyolitic dome; Figs. 2, 3e). The thickness of these volcanic rocks varies from a few tens to 500 m depending on their proximity to the effusive centers (Hadimi et al., 2018).

—U-Pb zircon ages by Sensitive High-Resolution Ion Microprobe (SHRIMP) on the Bled Mekrach garnet-bearing rhyolitic dome was recently performed by Hadimi et al. (2018): A concordant age obtained is 285.3 ± 4.9 Ma. More recent datings by Domeier et al. (2021) were performed on the andesite flow and andesite plug and yield $^{206}Pb/^{238}U$ ages of 284.2 ± 4.6 and 294.63 ± 0.67 Ma, respectively.

In the Mechraa Ben Abbou basin, 68 paleomagnetic cores at 11 different sites (5 of rhyolitic and two of andesitic geochemistry as well as 4 red bed sites) were drilled (Fig. S5, Table S5). Sites MEC1–3 and MEC10–11 all come from the Bled Mekrach garnet rhyolitic dome (Fig. 3e), which is why we assign an age of 285.3 ± 4.9 Ma (Fig. 2). At andesitic sites MEC4 and MEC5, direct contact to the basal conglomerates was identified, which stratigraphically ties them to the early phase of volcanism in MEC, which is why we assume by lithological correlation a mean age of 294.63 ± 0.67 Ma for them (Fig. 2). Additionally, an older paleomagnetic study from Westphal et al. (1979) documents two paleomagnetic sites in MEC (104 and 105) suspected to belong to the Mekrach rhyolitic dome complex and therefore assigned a provisional age of 285.3 ± 4.9 Ma (Table S5).

Eventually, since our red bed samples from MEC6–9 from the sedimentary record are stratigraphically bracketed by the basal andesitic lavas and the Bled Mekrach garnet rhyolitic dome, their deposition age is determined by these two magnetic pulses (Fig. 2; Table S5).

3.6. Chougrane-El had Bouhssoussene (CHO-BOUH)

The Permian volcanic Chougrane-El Had Bouhsoussene complex in the southern part of the Central Massif trends along a NE-SW oriented axis with an approximate length of 20 km and a maximum width of 8 km covering an area of about 110 km^2 (Figs. 1, S6; Domeier et al., 2021). The wedge shaped basin hosts a volcano-sedimentary succession with a thickness of about 180 m (Boutsougame et al., 2016). The BOUH-CHO basin was created by intracontinental transtensional tectonics in the Asturian phase during the late Carboniferous (Michard, 1976) and recorded two major eruptive episodes and a third phase dominated by dyke and sill emplacements. The eruptive episodes are represented by rhyodacites and overlaying basalts (e.g. Fig. 3f) which are intercalated in the reddish clay-sandstone-conglomeratic Permian deposits (Figs. 2, 3g, h; Boutsougame et al., 2016).

The basin can further be subdivided into spatially separated successions in the northeast (Bouhsoussene – BOUH) and the southwest (Chougrane – CHO). In this context, 66 paleomagnetic samples (volcanic rocks of various composition) were collected at 11 sites in BOUH whereas 100 paleomagnetic cores were retrieved at 14 sites (5 red beds, 4 sills and 5 volcanics) in CHO. Here, 94 out of 99 samples could be paleomagnetically measured (Tables S6 and S7).

The age of 270 ± 17 Ma of the BOUH-CHO complex is historically based on whole rock K—Ar data from volcanic rocks at Bir el Gassaa (Van Houten, 1976). Moreover, petrographic and geochronological characteristics of these effusives are comparable to those of the Cisuralian volcanic successions of KHE and TID (Hadimi et al., 2021; Youbi et al., 2018). On top of that, the volcanic pulses of CHO and BOUH can be temporally correlated via lithostratigraphy (Cailleux et al., 1983; Youbi, 1998). Recently, Domeier et al. (2021) reported geochronological data (although potentially affected by inheritance and Pb loss) from Bir el Gassaa (their sample TC1G) and Souk el Had Bouhsoussene (their sample TZ1G), which triggered some controversy about their respective eruption ages. TC1G provides age ranges of 307.8 ± 4 Ma to 295.5 ± 3.4 Ma. Inconsistent with its stratigraphic position, the TZ1G provides $^{206}Pb/^{238}U$ ages which span the Early and Middle Permian from 295.6 ± 2.9 to 267.9 ± 3.9. Thus, Domeier et al. (2021) concluded that these geochronological results might suggest that the Souk el Had Bouhsoussene sub-basin is younger than Chougrane therefore discounting the existing stratigraphic models.

Considering BOUH's available geochronological constraints (i.e. TZ1G), we can roughly attribute an intrusion age between 298.5 Ma and 264 Ma for our sites BOUH1–11 as well as paleomagnetic sites reported from the literature, i.e. Domeier et al. (2021; TZ1) and Daly and Pozzi (1976) (Table S7).

Apart from the geochronology sample TC1G from Domeier et al. (2021) only Van Houten (1976)'s whole-rock —K-Ar absolute age constraint (270 ± 17 Ma) is available for CHO clearly deviating from each other in absolute age. Since the latter's quality cannot be compared to modern standards, we are aware of its unreliable character and prefer to confine the emplacement of CHO's volcanic rocks using the available geochronological data from Domeier et al. (2021). Based on the considerations delineated above we assign an age range of 311.8–292.1 Ma to the volcanic sequences studied in CHO. This age also applies to earlier studies of the basin (Domeier et al., 2021; Westphal et al., 1979; see table S6). The red beds sampled in this study and by Daly and Pozzi (1976; their Série A) are estimated to belong to the Cisuralian, spanning 298.89–274.37 Ma according to Henderson et al. (2020).

3.7. Khenifra (KHE)

The 7 × 17 km large, SSW-NNE trending Khenifra basin is situated

Table 1
Summary of paleomagnetic results for the high-stability component (Component B). Age ranges are based on paleontological and geochronological constraints as presented in chapter 3 and were determined calculating the arithmetic mean of the age boundaries. See Tables S1–10 in the appendix for more information. n/N: number n of site-mean directions included in the determination of the basin-mean direction/number N of measured sites. Glat/Glong: Averaged geographic position of sampled basins given in latitude/longitude. Declination (Dec), Inclination (Inc) as well as statistical parameters after Fisher (1953), i.e. k (precision parameter) and α_{95} (angle of half cone of 95% confidence), of mean directions for all basins are given in geographic and stratigraphic coordinates whenever available. Plat/Plon show basin-specific paleopole positions calculated from paleomagnetic data in stratigraphic coordinates, whereas A95 and K are related Fisher parameters. References: Reference data added to this study's results, [1]: Domeier et al. (2021); [2]: Westphal et al. (1979); [3]: Daly and Pozzi (1976); [4]: Martin et al. (1978).

					Geographic coordinates				Stratigraphic coordinates				Pole position				References
Name	Age range [Ma]	n/N	Glat [°N]	Glong [°E]	Dec [°]	Inc [°]	α_{95} [°]	k	Dec [°]	Inc [°]	α_{95} [°]	k	Plat [°N]	Plon [°E]	A95 [°]	K	
Oued Zat (ZAT)	303.7–298.9	11/12	31.43	352.48	126	31.2	5.1	81.9	129.3	17.8	7.3	40	−26.8	51.3	6.8	46.4	–
Jebilet Massif (JEB)	290.5–259.6	4/5	31.89	351.65	123	−24.4	17.2	29.6	121.6	−16.9	14	44	−31.3	71.9	11.2	68.4	–
M'Tal (MTA)	290.5–274.4	6/7	32.45	351.64	128.1	−40.9	9	56.1	122.8	−4.2	8.6	62.1	−28.4	64.5	7.1	90.9	–
Nzalt-Lararcha (NL)	277.7–276.5	9/11	32.27	352.34	149.3	20.1	10.8	23.8	150.3	−12.6	11.7	20.4	−52.2	46.1	8.7	35.7	–
		12/14	32.27	352.35	146.5	22.6	8.9	24.9	149	−9.2	12	14.2	−49.8	45.3	8	30.4	[1]
Mechraa Ben Abbou (MEC)	293.3–283.1	10/11	32.64	352.23	147.8	−30	9	29.8	150.6	1.5	9.3	27.8	−46.5	37.9	7.5	43	–
	293.0–284.2	14/15	32.65	352.22	147	−32.6	7.2	31.8	147.8	1	7.6	28.4	−45	41.2	6.1	42.8	[1]
	292.8–284.0	15/17	32.65	352.22	–	–	–	–	147.7	0.5	7.1	30.1	−45.1	41.5	5.7	45.8	[1], [2]
Chougrane (CHO)	307.5–286.2	12/14	32.99	353.71	132.8	−1.1	10.9	16.7	133.2	−9.9	8.6	26.4	−38.3	61.5	7.3	36.7	–
	308.1–287.0	14/16	32.98	353.7	132.5	−0.7	9.6	18.3	132.8	−10.6	7.5	29.3	−38.2	62.2	6.3	40.3	[1]
	308.0–286.9	17/19	32.98	353.7	–	–	–	–	133.2	−9.7	6.2	33.9	−38.2	61.4	5.3	46.6	[1], [2], [3]
El Had Bouhssoussene (BOUH)	298.5–264	11/11	33.16	353.93	138.5	2.4	6.4	51.6	138.1	−7.3	5.4	73.1	−41.1	56.1	4	132.8	–
		12/12	33.16	353.93	139.4	2.2	6.1	52.3	139.4	−8.3	5.7	58.4	−42.4	55.4	4.5	95.3	[1]
		13/13	33.08	353.94	–	–	–	–	139.2	−8.1	5.3	62.7	−42.2	55.5	4.1	102.3	[1], [3]
Khenifra (KHE)	297.9–281.8	6/8	32.98	354.35	130.5	−13.5	7.8	73.9	128.6	−2.3	10.7	39.8	−32.3	62	7.4	83.8	–
	295.4–283.6	11/14	32.99	354.35	133.1	−10.5	9.6	23.8	132.4	−2.2	9.7	23.2	−35.2	58.9	8.2	32.3	[1]
	295.7–283.4	12/15	33.03	354.27	–	–	–	–	131.4	−1.7	9	24.1	−34.4	59.4	7.6	33.4	[1], [4]
Tiddas (TID)	290.6–275.7	11/11	33.62	353.8	149.6	10.6	8.7	28.6	149.3	−8.7	7.7	36.2	−49.1	45	6.9	44.7	–
	290.7–277.0	14/14	33.62	353.8	148.4	8.2	8.3	23.7	148.2	−6.8	7.2	31.4	−47.6	45.3	6.1	42.9	[1]
Bou Achouch (BOUA)	302.7–300.3	5/7	33.67	354.26	157.6	13.1	19.5	16.4	157.5	−0.5	22.8	12.2	−50.3	31	18.6	17.9	–
		6/8	33.67	354.26	159.9	13.5	15.9	18.8	159.1	1.6	18.5	14.1	−50.2	28.1	15	21	[1]

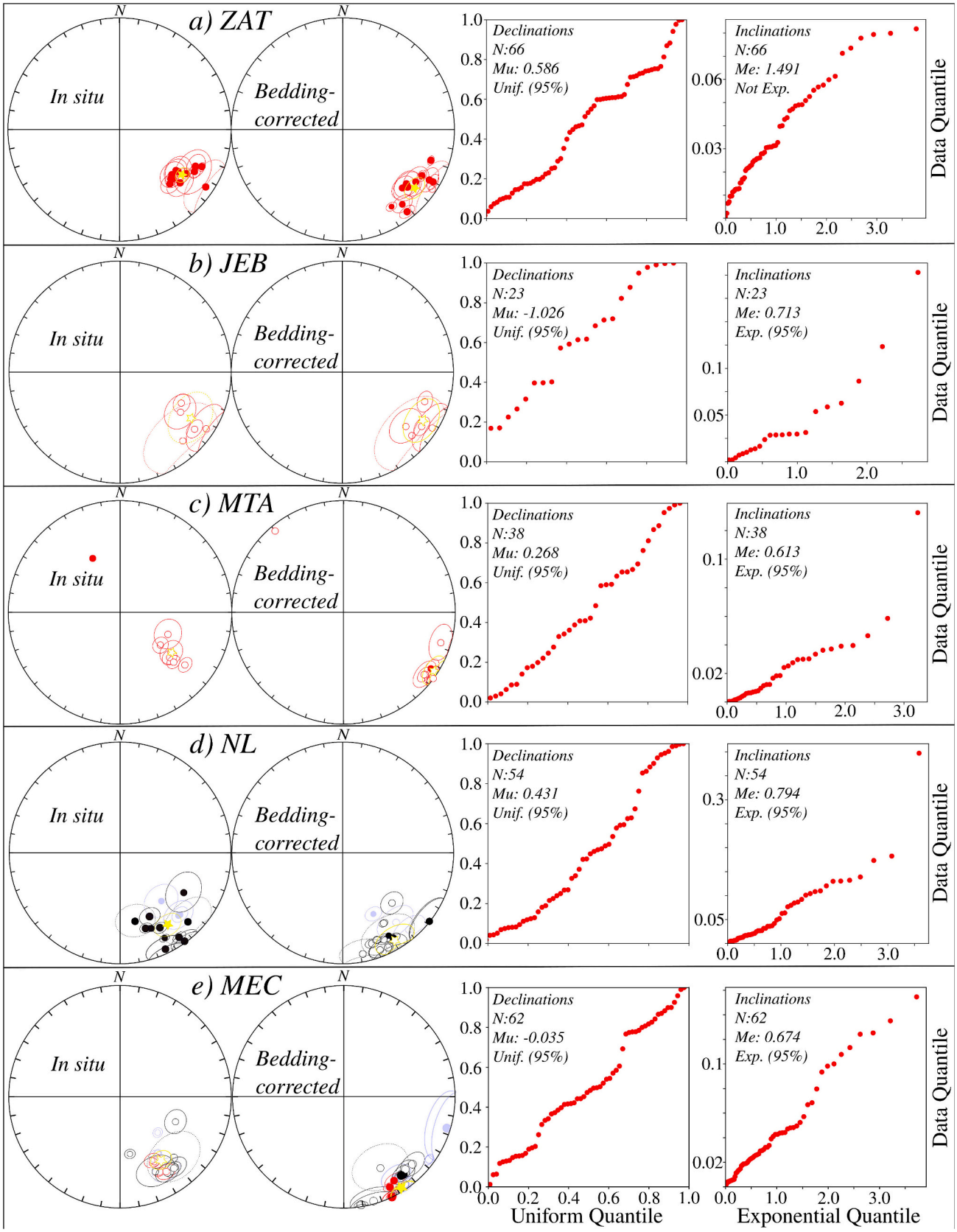

Fig. 7. Left panel - Stereographic equal-area projection of site-mean (circles) and basin-mean (yellow stars) directions in geographic (in situ) and tectonic (bedding-corrected) coordinates. Contours around the circles (stars) define the α_{95} Fisher (1953) angles of half cone of 95% confidence around the mean direction of respective sites (basins). Black (red) circles show site-mean stereographic projections of paleomagnetic data derived from volcanic (sedimentary) rocks whereas blue circles and 95% confidence ellipses reflect available data sets from the literature for respective basins. Data points with dotted contour lines have been discarded from further analysis when the reliability criteria of Van der Voo (1990) are not sufficiently met or respective data points are identified as outliers. Solid (open) symbols represent

projections in in the lower (upper) hemisphere, respectively. Numerical values for the shown data can be found in Table 1 and Tables S1–10 in the supplements. Right panel - Quantile-quantile diagram of declinations plotted against a reference uniform distribution (left) and inclinations drawn against an expected exponential distribution (right) taken from bedding-corrected paleomagnetic directions of this study's site-data after Fisher et al. (1993). If both test statistics M_u and M_e do not exceed the critical values of $M_u = 1.207$ and $M_e = 1.094$, the data is Fisher distributed at a 95% level of confidence. (For interpretation of the references to colour in this figure legend, the reader is referred to the web version of this article.)

about 160 km SE of Rabat in the eastern part of the Central Massif close to the western front of the Middle Atlas (Figs. 1, S7; Broutin et al., 1998; Voigt et al., 2011b; Youbi et al., 1995). KHE refers to a succession of red beds that unconformably rests on Hercynian basement of Ordovician to early Carboniferous age (Termier, 1936). El Wartiti et al. (1990) proposed a lithostratigraphic division of the Late Paleozoic deposits into three members of similar thickness: a) the lower member consists of stacked, coarse-grain dominated, fining-upward cycles whose conglomerates, sandstones, and few mudstones were probably accumulated in an alluvial-fan to alluvial-plain environment with major gradient changes (Fig. 3j). b) the middle member is characterized by a volumetric dominance of red and grey mudstones representing deposition on an extended floodplain. c) the upper member is located above an erosional unconformity indicating activation of the basin relief and begins with fluvial conglomerates; towards the top, fine-grained sandstones and pedogenetically overprinted mudstones become increasingly frequent. After red-bed deposition had ceased, first rhyolithic-rhyodacitic, then dacitic-andesitic flows were emplaced within the succession to form lower Permian volcanics that crop out in the center of the basin and along its north-western margin (Fig. 3i; Youbi et al., 1995). The whole section reaches an approximate thickness of 1800 m and is unconformably overlain by Late Triassic sediments (Fig. 2; Domeier et al., 2021 and references therein).

Macro- and microfloral remains in the middle part of the sedimentary succession of interbedded conglomerates, sandstones, and mudstones are supposed to be of middle to late early Permian age (Aassoumi et al., 1992; Broutin et al., 1998). More generally, the whole succession spans for most of the early Permian (Domeier et al., 2021).

The oldest volcanic pulse is represented by dacitic lava flows in the center of the basin at Taghat Hill and is dated by —U-Pb on zircon analysis to be 295.1 ± 2.9 Ma in age (Youbi et al., 2018). The composite volcanic dome of Sidi Tiri represents the largest occurrence of Permian volcanics in Morocco, crops out in the western part of KHE and unconformably overlies the Paleozoic basement. This complex made up of rhyolites, andesites and hybrid lavas yielded U/Pb SHRIMP ages ranging from 290.6 ± 2.6 Ma, 290.3 ± 2.1 Ma to 287.9 ± 3.8 Ma (Youbi et al., 2018). Finally, the emplacement of the last volcanic pulse (Talat Mechtal lava flows) capping the whole volcano-sedimentary succession can be bracketed between 282.76 ± 2.19 Ma (Domeier et al., 2021) and 280.3 ± 2.1 Ma (Youbi et al., 2018). In addition, reported ages of 305.59 ± 2.68 Ma (Domeier et al., 2021) or 264 ± 10 Ma (Jebrak, 1985) are either in conflict with the other age constraints or do not fulfil modern quality requirements.

In the Khenifra basin, 49 paleomagnetic cores at 8 sites (5 red beds and 3 rhyolites) were drilled (Fig. S7, Table S8). The sedimentary sites (KHE1–5 from this study and site M10 from Martin et al. (1978)) were sampled in lower Permian red beds that are capped by Talat Mechtal lava flows with an emplacement age of 280.57 Ma hence bracketing deposition between 298.89 Ma and 280.57 Ma (Table S8; Henderson et al., 2020).

Khenifra's oldest volcanic pulse, the dacites of Jbel Taghat Hill, have recently been dated 295.1 ± 2.9 Ma based on U—Pb on zircon analysis by Youbi et al. (2018). The rhyolitic samples KHE6–8 taken northwest of KHE's interior were dated 290.6 ± 2.6 Ma by a geochronological sample of Youbi et al. (2018) of the same section. The stratigraphy and position of KHE6, however, were difficult to estimate in the field (Fig. S7). Therefore, the paleomagnetic results from this site have been excluded (Table S8).

3.8. Tiddas-Souk Es-Sebt des Ait Ikko (Tsesdai / TID)

The Tiddas (TID) basin, about 110 km to the SE of Rabat, is located in the Khemisset region and represents the third largest Late Paleozoic continental trough in the northern Central Moroccan Meseta (Figs. 1, S8). It is about 20 km long and 2–3 km wide and shows a volcano-sedimentary reddish-violet succession of Permian rocks that rest unconformably on Visean marine sediments and are covered by Triassic and Cenozoic deposits (e. g. Cailleux et al., 1983; El Wartiti et al., 1990; Hadimi et al., 2021; Larhrib, 1996; Voigt et al., 2011a).

The cumulative maximum thickness of the Permian red bed succession has been proposed to range from 180 m (Aassoumi et al., 1992; Aassoumi and Vozenin-Serra, 1996; El Wartiti, 1981; El Wartiti et al., 1986; El Wartiti et al., 1990; Zouine, 1986) to 500 m (Broutin et al., 1998; El Wartiti, 1996) but was revised to not exceed 300 m (Larhrib, 1996). The stratigraphy of TID, generally incomplete due to faulting, is characterized by three red-beds formations (Hadimi et al., 2021; Larhrib, 1988; Larhrib, 1996): a lower formation (F1) represented by purple-red silty argillites, interbedded with polymictic, heterometric conglomerates, subhorizontal or cross-bedded sandstone and laminated to massive mudstones with minor intercalations of coal, limestone, and volcanic tuffs (Fig. 3k; about 100 m-thick); an intermediate formation (F2) consisting of planar to cross-bedded silty argillites alternated with channelized deposits (about 120 m thick) and an upper formation (F3) characterized by red silty argillites interspersed with sandstone (50 to 80 m-thick).

The Permian age of these formations was initially constrained using plant remains of early to late Permian affinities (Broutin et al., 1998). A recently described rich tetrapod footprint assemblage (Voigt et al., 2011a) ties the succession more precisely to the Artinskian –Kungurian (i.e. 290.51–274.37 Ma; Henderson et al., 2020) (Table S9).

The effusive and subintrusive magmatic units of TID consist of andesitic to dacitic flows and rhyolitic domes with associated rhyolitic dikes. In this context, three major volcanic pulses were distinguished (Hadimi et al., 2021): the first one (mainly andesitic) predates the Permian series; the second pulse is synsedimentary, displays different petrographic characteristics, and it is remarkable for its andesitic lava flows interbedded with the siliciclastic deposits. The third pulse of intrusive rhyolitic dikes is linked to the Ari el Mahsar rhyolitic dome emplacement and the dacitic flows. For the last volcanic pulse a concordant SHRIMP—U-Pb zircon age of 286.4 ± 4.7 Ma is also valid for our volcanic samples from TID (Fig. 2, Table S9; Hadimi et al., 2021).

In the Tiddas basin, we sampled 11 different sites (9 red beds and 2 andesites) and generated 73 drill cores, one drill core lost its orientation, which is why 72 paleomagnetic samples could be obtained for TID (Fig. S8, Table S9).

3.9. Bou Achouch (BOUA)

BOUA is a comparatively small (~1 km^2) basin located in the northeast of the Central Massif (Figs. 1, S9) and is represented by a 40 m thick volcano-sedimentary succession. It unconformably overlays the upper Visean-Namurian basement and is unconformably capped by Neogene deposits (Cailleux et al., 1983; El Wartiti et al., 1990).

Two groups of rocks can be distinguished: detritic rocks (conglomerates, silt- and sandstones) and volcanic rocks with calc-alkaline affinity (andesites and rhyolites). The latter crops out in different ways: as lava flows, pyroclastic deposits (e.g. tuffs) and dikes. The petrographic characteristics of the Carboniferous volcanic rocks of BOUA show great similarities with those of TID (El Wartiti et al., 1990) and KHE (Youbi,

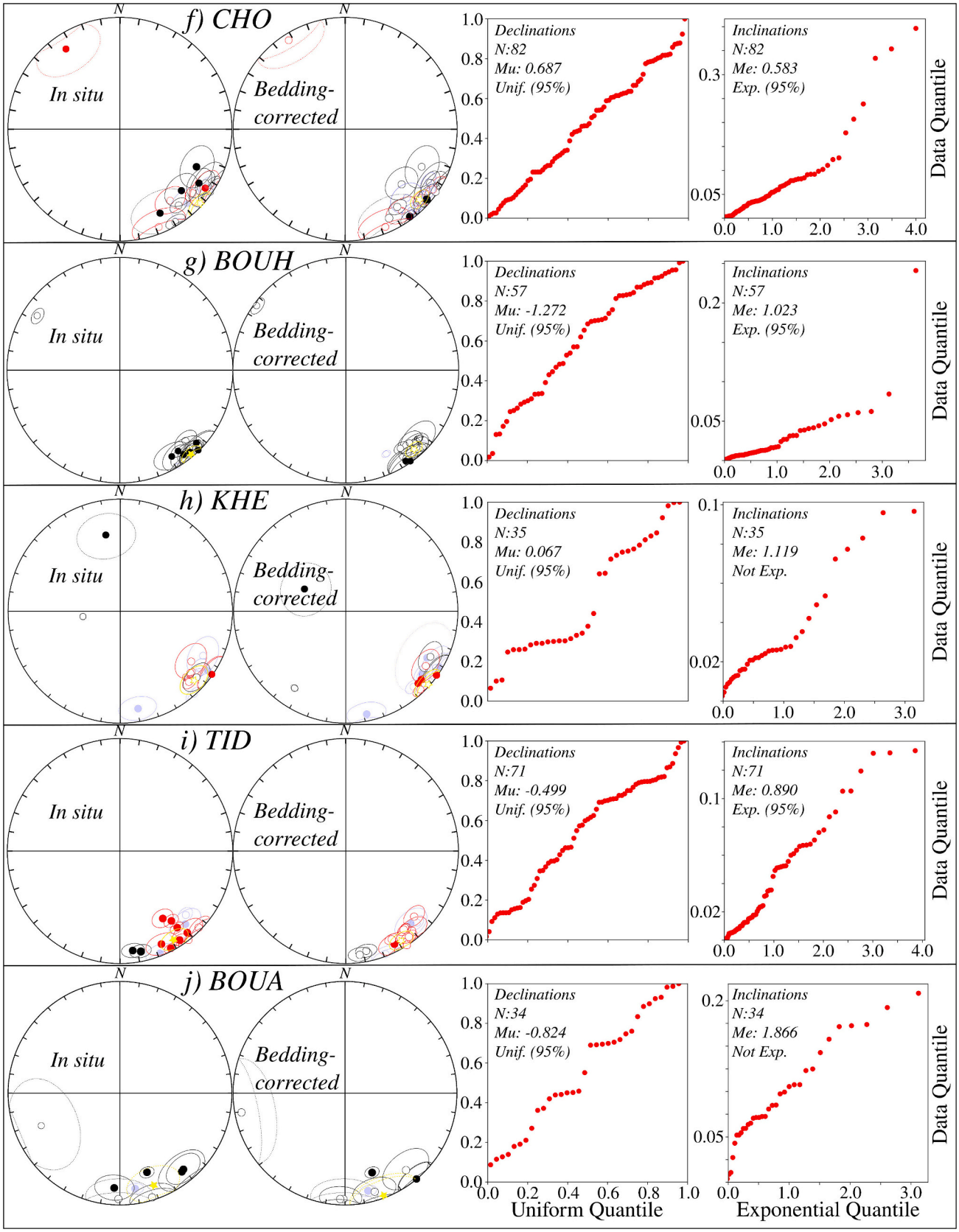

Fig. 7. (*continued*).

1998). A first volcanic episode (mainly rhyolites) crops out in the NE part together with cinerites and fine-grained sediments (El Wartiti et al., 1990). They are overlain by coarser-grained deposits, rich in volcanic pebbles. At the top of the succession a mainly andesitic volcanic episode occurs (Fig. 2).

A rich macroflora assemblage was recovered from the finer grained clastic units (Broutin et al., 1998) permitting to link these sediments to the Kungurian. Subsequently, Kerp et al. (2001) shifted this age constraint to the latest Carboniferous on the basis of similarities between the BOUA floras and those of the Lower Rotliegend of the Saar-Nahe Basin in Germany. The only available geochronological constraint from BOUA includes zircons where ~60% have ages which cluster around 300 Ma, and the youngest part of this cluster provides a weighted mean $^{206}Pb/^{238}U$ age of 301.50 ± 1.24 (Domeier et al., 2021). This latest Carboniferous age supports the observations of Kerp et al. (2001) and is therefore esteemed more realistic than the earlier postulated Kungurian age.

In the basin of BOUA, we drilled 50 cores at seven sites, of which three were extracted from rhyolites and cinerites (tuff), respectively (Fig. S9, Table S10). Since the only available absolute age constraint is reported by Domeier et al. (2021) to be 301.50 ± 1.24 Ma, a corresponding age range is assumed for all studied sites (Table S10).

4. New paleomagnetic data

4.1. Methodology

All samples were extracted using a portable petrol-powered water-cooled rock-drill and oriented with a standard magnetic Brunton compass and an inclinometer in the field. Then, they were cut into cylindrical specimens of about 1-in. diameter and a volume of about 10 cm^3 at the Department of Earth and Environmental Sciences of the Ludwig-Maximilians-University of Munich. When possible, several specimens from one sampled core were generated and labelled alphabetically from the top to bottom of the core. Broken specimens have been fixed with heat-resistant, non-magnetic glue. Finally, they have been subjected to demagnetization and paleomagnetic measurements in a magnetically shielded room in the Department of Earth and Environmental Sciences in Munich.

After detailed pilot studies applying alternating field (AF) and thermal demagnetization procedures, most of the samples were thermally demagnetized using an ASC oven (ASC Scientific Model TD-48, Thermal Specimen Demagnetizer). Paleomagnetic measurements were carried out using the SushiBar, an automated sample handling system integrated with a three axis, 2G Enterprises superconducting rock magnetometer (Wack and Gilder, 2012). After each heating step, the specimens were allowed to cool down in magnetically field free space and their remanent magnetization was measured on the three axis 2G cryogenic magnetometer.

Paleomagnetic data analysis was carried out using an online, open source multi-platform tool (Paleomagnetism.org - Koymans et al., 2016, Koymans et al., 2020) and the software Palaeomag-Tools from Hounslow (2006). Directional data is presented via orthogonal vector diagrams (Zijderveld, 1967) on equal area projections and analyzed by applying a least square method (Kirschvink, 1980) on linear parts of the demagnetization plots defined by a minimum of four consecutive demagnetization steps. The linear segments were anchored to the point of origin when appropriate. Subsequent statistical analysis of the results was carried out after Fisher (1953) and includes calculation of mean directions as well as virtual geomagnetic poles and paleopoles. Furthermore, parametric bootstrap fold tests (Tauxe and Watson, 1994), incremental fold tests (Watson and Enkin, 1993) and inclination-based fold tests (based on "inclination-only" and "block-rotation fisher"-BRF analysis) (Enkin and Watson, 1996) have been routinely applied to all site mean data. In addition the data sets have been subjected to the quantile-quantile method (Fisher et al., 1993) in order to test whether the respective paleomagnetic data fulfils the criterion of a Fisher distribution. For further visualisation of acquired data in shown figures, GMAP2015 (Torsvik et al., 2015), GMT (Wessel et al., 2019) and GPlates (Müller et al., 2018) have been utilized.

In order to check the magnetic mineralogy, rock magnetic measurements were conducted on leftovers of the paleomagnetic samples (at least one per site with 5 mm diameter). Hysteresis loops, backfield curves and thermomagnetic curves were determined for each of the sites using an MM VFTB (Munich Measurement Limited Variable Field Translation Balance; Krása et al., 2007) and a one-component Lakeshore Vibrating Sample Magnetometer (VSM) (general principle after Foner, 1959). Additionally, an isothermal remanent magnetization (IRM) of up to 2.5 T was imparted on selected samples using a MMPM10 Pulse Magnetizer. The rockmagnetic data was visualized with a custom-made MATLAB code.

4.2. Results

4.2.1. Rock magnetic results

Since the rock-magnetic behaviour is not basin-specific but lithology controlled, we split the 97 sampled sites into groups of characteristic rock types (Fig. 4). 50 sites (from seven basins) from volcanic rocks are subdivided into mafic outcrops (group I), rhyolitic rocks (group II) and two endmembers for andesitic samples (groups III and IV). Another 47 sites (from seven basins) are from sedimentary rocks, mostly medium-grained red beds (group V).

Mafic samples display sharp-shouldered hysteresis loops indicative of a single low-coercivity ferrimagnetic component (Fig. 4 Ic), IRMs with sharp increase up to 100 mT and approximate saturation at 1 T (Fig. 4 Ib) and thermomagnetic curves with steady loss of magnetization and unblocking temperatures at ~580 °C and occasionally around 200 °C (Fig. 4 Ia) reflecting the occurrence of magnetite as the main magnetic carrier and potential relevance of maghemite in minor proportions.

The group of rhyolites shows broadly shouldered and wasp-waisted hysteresis loops (Fig. 4 IIc) and IRMs with steep magnetization increase up to 100 mT followed by a gradual increase up to 2.5 T without reaching saturation (Fig. 4 IIb) hence pointing towards presence of a high and a low coercive magnetic mineralogical component. Corresponding thermomagnetic curves mostly show a distinct inflection of the heating branch at around Tc1 ~ 580 °C, a less pronounced intensity drop at Tc2 ~ 650° as well as a much lower magnetization acquisition during cooling below 570 °C (Fig. 4 IIa). This probably reflects a potential breakdown of primary maghemite to hematite plus presence of magnetite and hematite as magnetic carriers.

Andesitic specimens reveal a broad spectrum of rockmagnetic properties and typical endmember cases (groups III and IV) are shown in Fig. 4. On the one hand, most of the andesites are characterized by wasp-waisted hysteresis loops (Fig. 4 IIIc), IRM curves with a steep increase in magnetic intensity up to 100mT and then a gradual increase up to 2.5 T without saturating (Fig. 4 IIIb) and reversible thermomagnetic curves with two distinct inflections at Tc1 ~ 570 °C and Tc2 ~ 680 °C (Fig. 4 IIIa) suggesting alternating combinations of magnetite and hematite. On the other hand, a significant part of the andesitic volcanic rocks exhibits wide-shouldered hysteresis branches (Fig. 4 IVc), IRMs with steady increase in magnetization approaching saturation at 2.5 T (Fig. 3 IVb) and reversible thermomagnetic curves with Tc ~ 660 °C (Fig. 4 IVa) which we ascribe to sole prevalence of hematite in these samples. Similar rock-magnetic findings for early Permian andesites from Morocco are also reported by Domeier et al. (2021).

The rock-magnetic properties of the red beds are mostly dominated by wide-shouldered hysteresis loops (Fig. 4 Vc) with high coercivities, IRMs with almost no magnetization acquisition up to 250 mT and a subsequent steady increase up to 2.5 T without reaching saturation (Fig. 4 Vb) and reversible thermomagnetic curves with a distinct inflection around Tc ~ 650–660 °C. Additionally, low and medium temperature components are present to a minor extent (Fig. 4 Va). The red

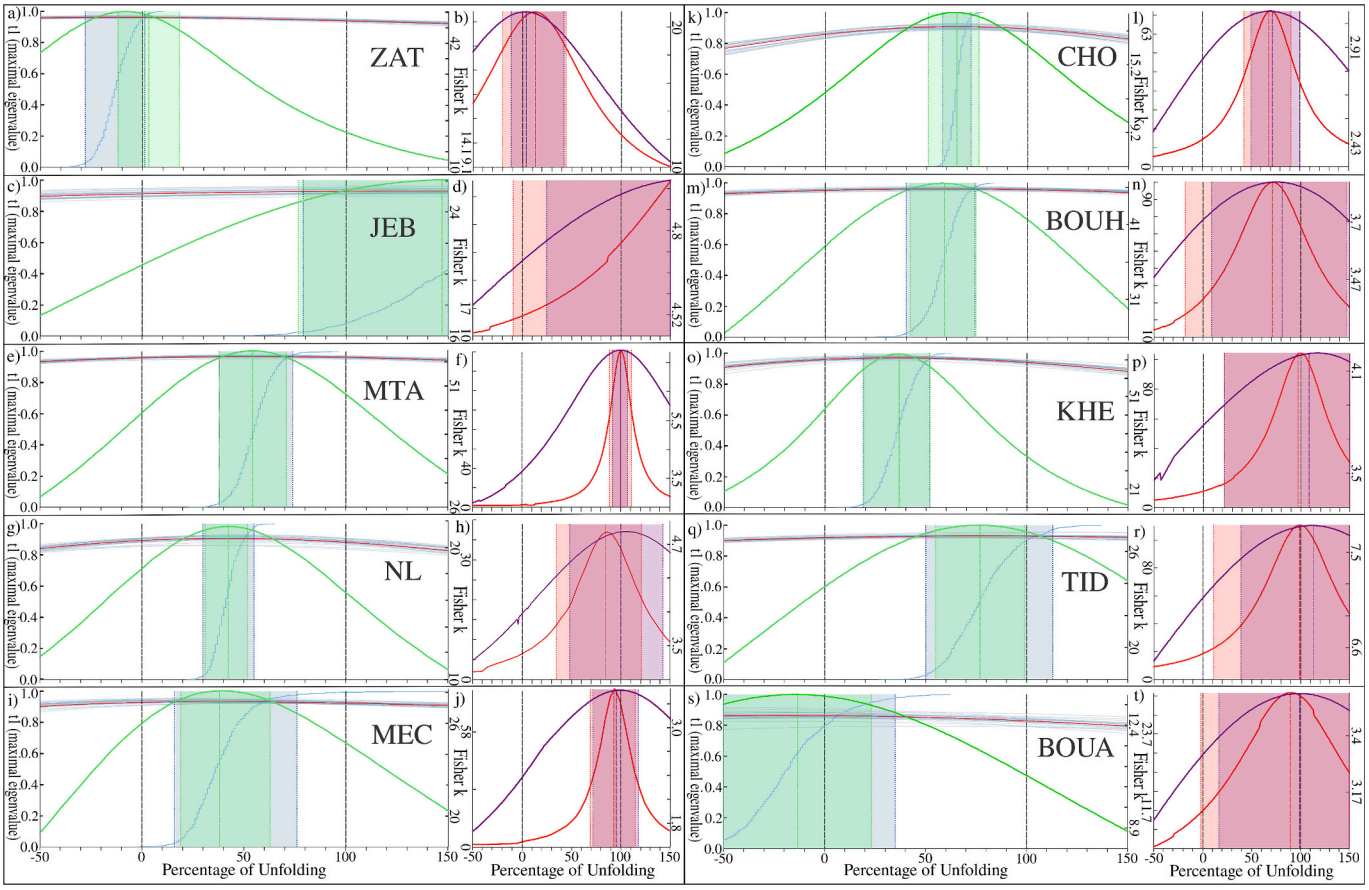

Fig. 8. Fold tests applied on component B data from this study arranged according to sampled basins from south to north. Threshold values of geographic coordinates/no folding (0%) and tectonic coordinates/complete folding (100%) are given by black vertical dashed lines. Left panels (a, c, e, g, i, k, m, o, q, s): Application of the parametric bootstrap fold test (blue) after Tauxe and Watson (1994) with $N = 1000$ iterations and corresponding τ_1 eigenvalues (left ordinate) plotted against percentage of gradual unfolding. Red curves mark τ_1 values of the non-bootstrapped data and respective light blue curves represent the first 25 bootstrapped curves. 95% confidence intervals are highlighted by blue shaded intervals delimited by stippled vertical lines and cumulative density functions (CDFs) are represented by the blue curves. Fisher precision parameter k (right ordinate) is plotted against percentage of unfolding according to the incremental fold test procedure (green curve) as suggested by Watson and Enkin (1993) using 1% of incremental change in dip per iteration step. Best groupings of k are represented by dashed green vertical lines, with 95% confidence intervals shown as green shaded interval confined by green dotted vertical lines. Right panels (b, d, f, h, j, l, n, p, r, t): Results of inclination-based fold tests following Enkin and Watson (1996) where k is plotted against the percentage of unfolding. In the case of the inclination-only approach (red curve), maximal clustering of k (left ordinate) is characterized by the red dashed vertical lines, respectively, whereas corresponding 95% confidence intervals (determined by parametric simulation) are depicted by reddish areas delimited by red dotted vertical lines. For fold tests based on block-rotation fisher (BRF) analysis (purple curve), maximal values for k (right ordinate) are visualized by purple dashed vertical lines, respectively. Associated 95% confidence intervals (also based on parametric simulation) are indicated by purple areas confined by purple dotted vertical lines. (For interpretation of the references to colour in this figure legend, the reader is referred to the web version of this article.)

bed's magnetic mineralogy is therefore characterized by predominance of hematite with the addition of minor amounts of goethite and potentially pyrrhotite.

4.2.2. *Paleomagnetic results*

4.2.2.1. Demagnetization behaviour of the NRM. Fig. 5 shows representative orthogonal projection diagrams (Zijderveld, 1967) of all sampled basins and lithologies sorted from South to North according to the geographic position of the basins shown in Figs. 1 and 2. Since AF demagnetization experiments on pilot samples rendered either ineffective due to high presence of hematite within the sampled basins (Fig. 4) or produced comparable results to its heated counterpart (e.g. Fig. 5e vs. Fig. 5f), thermal demagnetization was predominantly used to isolate characteristic directions of the NRM.

While some samples exhibit straightforward unidirectional behaviour (Fig. 5a, e, f, g), the majority is characterized by two distinct directional components, where the Low Temperature Component (LTC) or Component A, is typically isolated below 300 °C and covers variable proportions of the respective NRM (Fig. 5b, c, d, h-l). Upon further demagnetization, intensity of the High Temperature Component (HTC) or Component B is gradually removed and trajectories of the magnetic vectors trend towards the origin while trespassing unblocking temperatures corresponding to the underlying rockmagnetic mineralogy (Fig. 4). Accordingly, a "hematite unblocking spectrum" between 625 °C and 700 °C can be observed in the red beds (Figs. 5a-c). Demagnetization ranges diagnostic for magnetite characterize the mafic volcanic rocks (Fig. 5g) and some rhyolites (Fig. 5f and j). A broader unblocking interval is evident for rhyolites and andesitic sills linked to a higher amount of hematite (Fig. 5i and l). Ultimately, all andesites are associated with a striking unblocking spectrum at high temperatures beyond 625 °C indicating prevalence of hematite and unblocking spectra of differing width at intermediate temperatures between 450 °C and 575 °C highlighting variable influence of magnetite (Fig. 5d, e, h, k).

Notably, demagnetization behaviour of both HTCs is not significantly varying across the sampled basins, where both components (magnetite and hematite related) are more or less collinear. Almost all of the samples are of reversed polarity consistent with their suggested late

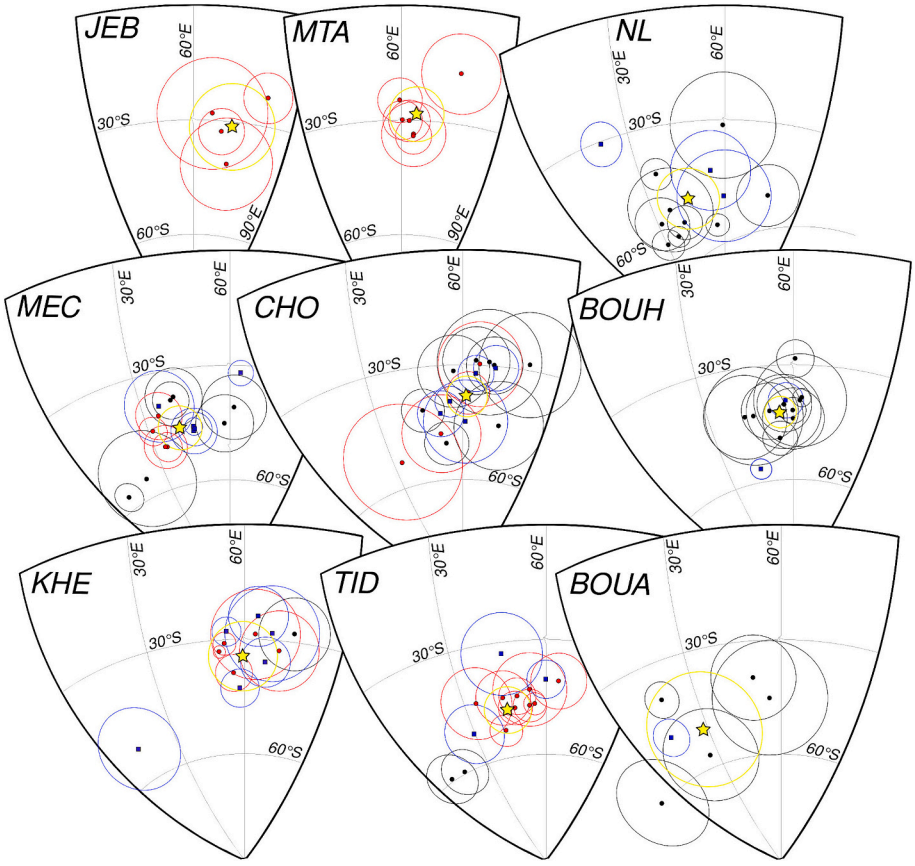

Fig. 9. Virtual geomagnetic poles from the primary high stability components of this study (red dots – red beds, black dots – volcanics) and of comparable literature (blue squares) with constituent uncertainties in tectonic coordinates in a Mesetian reference frame. For each basin, a paleopole and corresponding A95 (yellow star and contour) was calculated. Numerical values can be found in Table 1. (For interpretation of the references to colour in this figure legend, the reader is referred to the web version of this article.)

Carboniferous to early Permian age which falls within the Kiaman reversed superchron spanning from the mid-Bashkirian (about 318 Ma; Aretz et al., 2020; Hounslow, 2022) to the early Wordian (around 267 Ma; Hounslow and Balabanov, 2018). However, a small number of drill cores (11 samples from 3 sites in total) are characterized by a strong and stable remanence of normal polarity (Fig. 5g), which can be correlated to one of the normal magnetozones within the Kiaman reversed superchrone (Hounslow and Balabanov, 2018).

4.2.2.2. Mean directions. Component 'A' mean directions and their averaged overall mean direction are clustering around the recent geomagnetic field for the sampling area (D = 358.4°, I = 44.1°; using IGRF2020 model: https://www.ngdc.noaa.gov/geomag/calculators/magcalc.shtml#igrfwmm from July 20th, 2022) and is therefore interpreted to be of secondary origin (Fig. 6).

The high stability component or component 'B' is generally falling within the southeastern quadrant of the stereographic equal-area projection, with declinations ranging from ESE to S and shallow to moderate inclinations that are rotated towards the horizontal upon applying tectonic correction thereby minimizing potential inclination shallowing effects. Mean directions of Late Paleozoic Moroccan sites and basins from this study as well as available literature data reported by Daly and Pozzi (1976), Martin et al. (1978), Westphal et al. (1979) and Domeier et al. (2021) are listed in Table 1, Tables S1-S10 in the supplements and shown in the left panel of Fig. 7.

Some site mean directions (MTA1, CHO1 and BOUH2) point down and towards NW, antipodal to the dominating SE and up component observed elsewhere (Fig. 7c, f, g). While MTA1 consists only of one paleomagnetic direction and CHO1 is poorly constrained (α_{95} = 20.3°), BOUH2 displays a well-defined (α_{95} = 4.9°, k = 244.6) site mean-direction (D = 303.4°, I = −13.7° in geographic coordinates and D = 306.1°, I = −3.7° in tectonic coordinates) which should reflect a geomagnetic reversal.

A conspicuous feature also noticed by Domeier et al. (2021) in their data set is the elongation of the site-mean declinations along small circles in most of the basins after tilt-correction (Fig. 7). Since there is no systemic directional difference between red beds and volcanics and both groups seem to be equally streaked, this rotational effect is no sedimentary feature but might rather reflect vertical axis rotations given the transpressive tectonic regime and abundance of dextral fault zones in the sampling area (chapter 3). Rotated/elongated paleomagnetic data typically miss characteristic attributes of a Fisher distribution, revealed by the quantile-quantile method of Fisher et al. (1993) (right panel of Fig. 7). Site-mean directions of three basins (ZAT, KHE and BOUA) are not Fisher distributed, whereas NL and MEC statistically fulfill the requirements of a Fisher distribution but their tendency to form a girdle is visually evident (Fig. 7d and e). For the remaining basins, Fisher parameters improve after bedding-correction on the 95% significance level.

4.2.2.3. Fold tests. In order to constrain component 'B's relative magnetization age and to further investigate the potential influence of vertical axis rotations on our data set, we conducted an incremental fold test after Watson and Enkin (1993), a parametric bootstrap fold test (Tauxe and Watson, 1994) – hereafter called 'bulk fold tests" – as well as inclination-based fold tests following Enkin and Watson (1996), namely the inclination-only approach and BRF analysis, for every basin (Fig. 8). In general, the fold tests show similar behaviour and can be subdivided

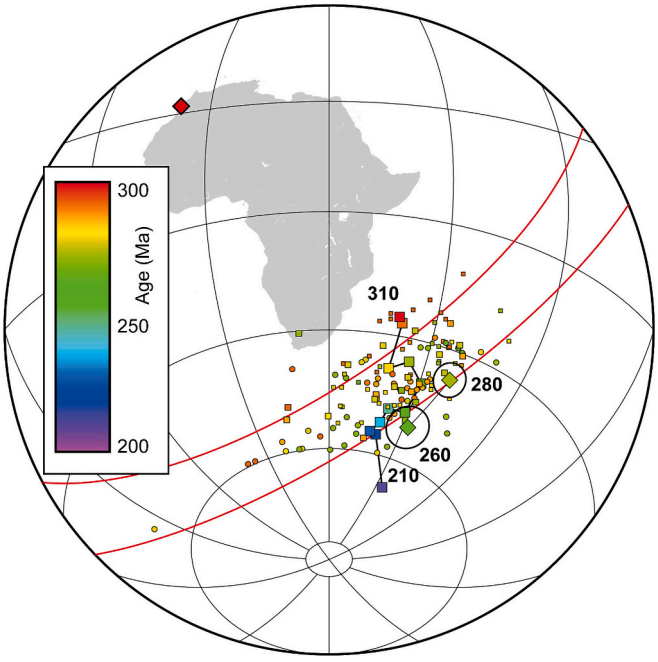

Fig. 10. Virtual geomagnetic poles from this study (circles) and VGPs from current literature (squares) plotted in combination with 260 Ma and 280 Ma mean paleopoles (diamonds with black A95 confidence ellipses) from Channell et al. (2022) and the 310 Ma to 210 Ma APWP of Gondwana (big squares) by Torsvik et al. (2012). 95% confidence ellipses for this study's VGPs and for the APWP of Gondwana are not shown for clarity. All poles are colour-coded according to their estimated mean ages (time bar from 300 Ma to 200 Ma shown in inset for comparison). Most poles fall within a small circle swath confined by red lines intersecting the Gondwana APWP at a time window of 300 Ma to 260 Ma. The pole of rotation to the small circle band is the sampling area (big red diamond) within the northwest of Africa (grey contour). (For interpretation of the references to colour in this figure legend, the reader is referred to the web version of this article.)

into four different categories.

In the first group, all fold tests rendered negative which only comprises the southernmost sampled basin ZAT (Fig. 8a and b). Secondly, areas JEB and TID exhibit positive parametric bootstrap fold tests (Fig. 8c, q). The incremental and inclination-based fold tests yield an improved clustering of directional data upon untilting (i.e. a significant increase in k from 0% to 100% unfolding) for both basins. The incremental fold test for JEB also yields a formally positive result (Fig. 8c), whereas the incremental fold test for TID renders inconclusive with 95% confidence intervals at 55% and 99% unfolding (Fig. 8q). The inclination-only fold test for JEB is marked by large confidence intervals including both the 0% and 100% threshold value potentially due to the low number of samples for this basin, while the BRF fold test for JEB as well as both inclination-based fold tests for TID are positive (Fig. 8d and r). The third category comprises all basins of the Rehamna massif (MTA, NL and MEC) and the southern basins of the central massif (CHO, BOUH and KHE). All bulk fold tests turned out inconclusive with *syn*-folding maximal clustering at intermediate percentages of unfolding (Fig. 8e, g, i, k, m, o; Tables S3-S8) in accordance with the inconclusive regional fold test of Domeier et al. (2021). As pointed out by Domeier et al. (2021), since the folding within the basins should be related to the final phases of the Variscan orogeny, a syn-folding maximal clustering would imply a paleomagnetic signal not much younger than the primary ca. 280 Ma ages. However, in contrast to their also inconclusive regional inclination-only fold tests, the inclination-based fold tests of MTA (Fig. 8f), NL (Fig. 8h), MEC (Fig. 8j) and KHE (Fig. 8p) of this study are positive with varying widths of their respective confidence intervals implying a primary character of the magnetization and post-depositional variations of the declinations. For BOUH and CHO, at least their BRF fold tests were positive, while their inclination-only fold tests were either inconclusive or accompanied by huge uncertainty intervals albeit clearly showing an increase in k upon unfolding (Fig. 8l, n). Ultimately, the northernmost sampled basin BOUA exhibits negative bulk fold tests, but a distinct increase of directional grouping for both inclination-based fold tests when reaching 100% unfolding, thereby providing a positive BRF fold test and a formally inconclusive inclination-only fold test due to its large 95% confidence interval most likely related to the comparatively low number of available samples from BOUA (Figs. 8s-t).

4.3. *Discussion of the new paleomagnetic data*

For the southernmost basin ZAT all fold tests are negative (Fig. 8a and b), Fisher parameters deteriorate after applying tectonic correction (Table 1) and resulting paleolatitudes rather fit the ~260 Ma segment of the APWP of Gondwana than its assigned late Carboniferous age (Fig. 11), suggesting that ZAT represents a late Permian remagnetization and is therefore no longer considered in this work.

For each of the remaining nine basins, at least one of the bulk or inclination-based fold tests yields positive results (Fig. 8), indicating their high stability components to be primary. Further support for this interpretation comes from the identification of normally magnetized samples/sites at three different sites/basins (i.e. MTA1, CHO1 and BOUH2). While MTA1 (N = 1) and CHO1 (α_{95} = 20.3°) are admittedly associated with some uncertainty (Fig. 7c and f; Tables S3 and S6), BOUH2 is well-defined and unequivocally represents a reversal (Fig. 7g, Table S7). Since it is expected that the volcanics of BOUH were emplaced between 298.5 Ma and 264 Ma (Table S7), we ascribe the reversal to one of the two well-documented short normal magnetochrones CI2n (281.24 ± 2.3 Ma) or CI3n (275.86 ± 2.0 Ma) within the Kiaman reversed superchrone (Hounslow and Balabanov, 2018). Domeier et al. (2021) also describe data (LTC of their site TZ1) hinting towards the possibility of a reversal within BOUH. If the reversal character of MTA1 and CHO1 is presumed and their estimated age range is considered (Tables S3 and S6), both sites can be ascribed to CI2n or CI3n. Relative and absolute age constraints favour CI2n (281.24 ± 2.3 Ma) as temporally closest (late-Artinskian) and therefore representative magnetochrone for all three sites (chapter 3), but we emphasis the preliminary character of this interpretation.

5. Summary of paleomagnetic data from Morocco

5.1. *Virtual Paleomagnetic Poles*

To properly investigate the large amount of paleomagnetic data and its impact on paleogeographic reconstructions, all primary site/basin mean directions from this study (red/black circles for red beds/volcanics) and from available literature (blue squares) were transformed into virtual geomagnetic poles (VGPs; Fig. 9). Therefrom, paleopoles were calculated for each basin (yellow stars) which are also listed in Table 1. In accordance with the findings of section 4.2.2, no striking difference between samples of sedimentary and volcanic origin was found thus further corroborating the hypothesis that inclination shallowing is widely absent in our sedimentary samples.

A majority of the inspected basins show an elongation of their bedding corrected VGPs in NE-SW direction, an observation also reported by Domeier et al. (2021) for their significantly smaller Moroccan data set, who also suggest relative vertical axis rotations between or within constituent basins as a potential cause. Hence, in order to reliably assess and identify systematic rotational displacements, the data set needs to be discussed on a site-specific and basin-specific level. Therefore, we plotted all available primary Late Paleozoic Moroccan VGPs from the present study and from the literature on site-level with their respective mean ages against the 310 Ma – 210 Ma APWP of Gondwana

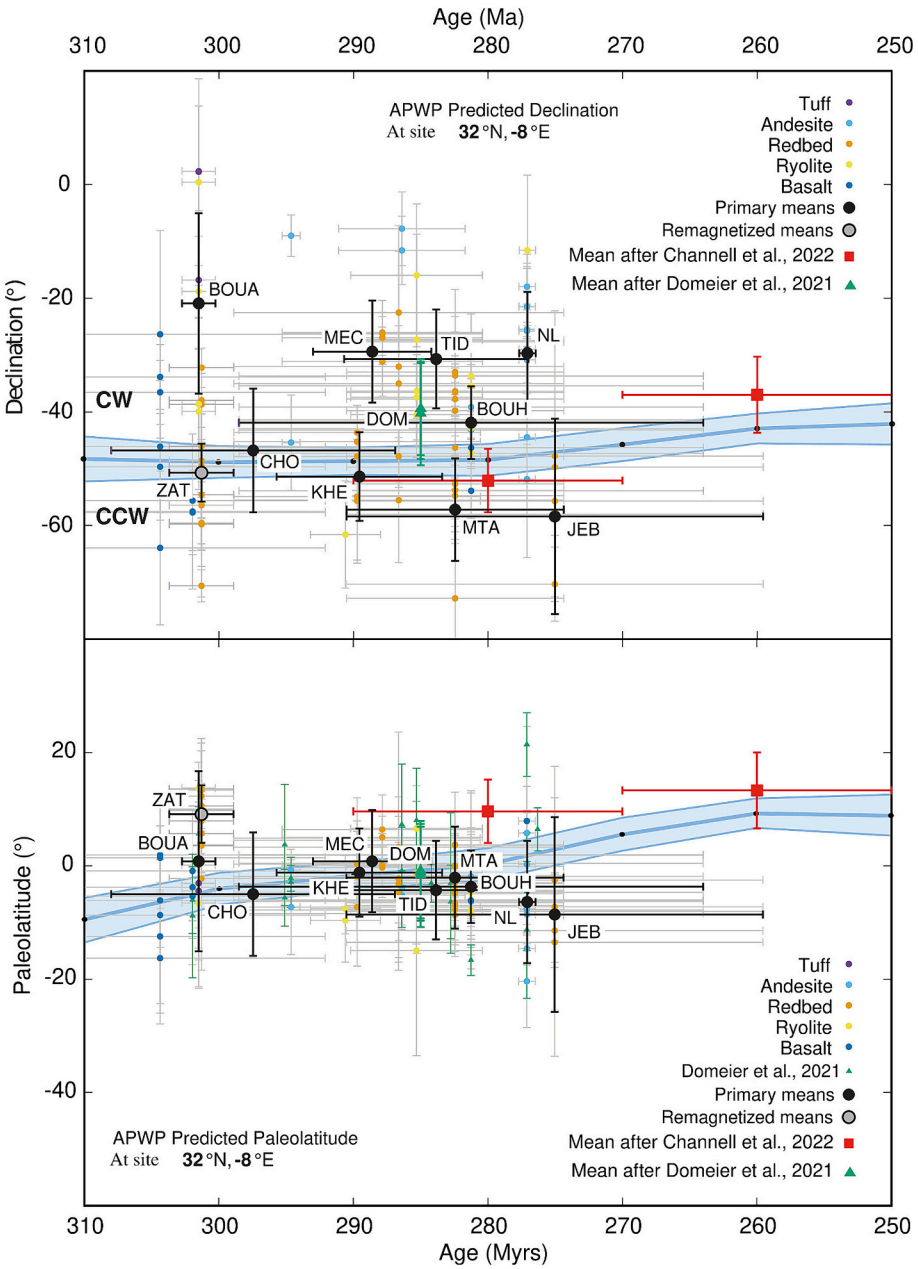

Fig. 11. Declination and paleolatitude drawn against assigned age ranges (with error bars) for the Moroccan results of this study on site-level (circles colour-coded according to underlying lithology) and basin-level (big black circles) as well as of Domeier et al. (2021) (green triangles) and of Channell et al. (2022) (red squares). The grey and black contoured circles show the mean of the putatively remagnetized site ZAT. Predicted declination and paleolatitude values based on the Gondwana APWP of Torsvik et al. (2012) and Channell et al. (2022) calculated for a nominal reference point amidst the sampled area in Morocco at 32°N and -8°E (blue polygon with associated error band). (For interpretation of the references to colour in this figure legend, the reader is referred to the web version of this article.)

(Torsvik et al., 2012) to obtain a more comprehensive picture (Fig. 10).

The VGPs from this study and published poles of comparable age for Morocco are broadly spread along a small circle band about a rotation point in Morocco and intersect the early Permian segment of the APWP. Moreover, the VGPs are plotting on both sites of the APWP, with an emphasis rather to the SW. These observations are in agreement of various amounts of vertical axis rotations affecting the Moroccan paleomagnetic dataset. Apparently, counter-clockwise (ccw) and – to a higher percentage – clockwise (cw) vertical axis rotations are recorded in the studied samples, at least on site-level, with respect to Gondwana.

To further investigate the potential influence of rotational movements on basin-level and its dependence on lithology, Fig. 11 shows all declinations and calculated paleolatitudes of site-mean VGPs and basin-mean paleopoles from this study as well as from published data sets drawn against their corresponding mean ages with uncertainties and colour-coded according to their lithology (see legend). The expected declinations and paleolatitudes for a nominal reference point (Glat = 32°N, GLon = −8°E) were calculated based on the paleomagnetic compilations of Torsvik et al. (2012) and Channell et al. (2022). While a separate behavior is not detectable for volcanic and sedimentary results in Fig. 11, prominent features become obvious for both declination and paleolatitude subplots entailing further implications on rotational mechanisms and paleogeographic reconstruction of the Moroccan Meseta.

5.2. *Declination variations and rotational mechanism*

Whereas the expected declination from the APWP of Gondwana

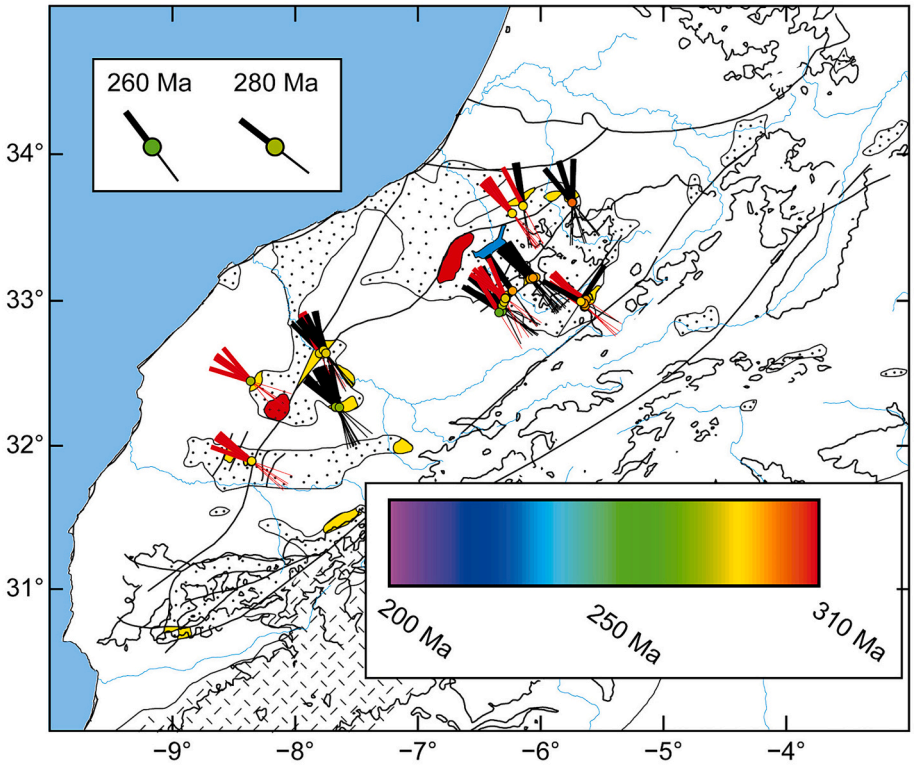

Fig. 12. Declination values at the respective sites and basins shown with underlying main geologic units of Fig. 1. Reference declination at 260 Ma and 280 Ma are given in the top left of the figure for comparison. Fat black (red) lines display orientation of the volcanic (red bed) site mean declinations while colour of the corresponding circle indicates the basin-mean age. (For interpretation of the references to colour in this figure legend, the reader is referred to the web version of this article.)

Table 2
Paleomagnetic poles used for reconstructions:

Area	Lat N	Long E	A_{95}	Reference
Gondwana[1] (GP2)	−37.7	59.3	6.1	(Domeier et al., 2021)
Laurussia[1]	−45.0	340.9	2.6	(Torsvik et al., 2012)
Gondwana[2]	−41.5	62.3	3.8	(Channell et al., 2022)
Laurussia[2]	−46.0	345.1	2.7	(Channell et al., 2022)
JEB	−31.3	71.9	11.2	This study
MTA	−28.4	64.5	7.1	This study
NL	−49.8	45.3	8	This study
MEC	−45.1	41.5	5.7	This study
TID	−47.6	45.3	6.1	This study
BOUH	−42.2	55.5	4.1	This study
KHE	−34.4	59.4	7.6	This study

Lat N, Long E: paleopoles latitude and longitude in ° north and east. A_{95}: confidence interval.

would suggest values between −40° and − 60°, the Moroccan data reveal a large spread of declination between 0° and − 60° with deviations up to 40°- 50° (Fig. 11). Upon calculation of basin-mean values, the spread decreases but is still statistically significant compared to predicted declinations. A clear trend of declination versus age, i.e. a proportionality of increasing age and declination deviation, is absent with only the northernmost and oldest basin BOUA showing the highest ΔD. In sum, the predominance of cw rotations with respect to the referential APWP is observed both on site-level and basin-level.

The calculated declination based on the Meseta paleopole of Domeier et al. (2021) is located in the middle of this study's declinations based on our basin-mean paleopoles. The results of Domeier et al. (2021) only exhibit a slight amount of rotation within error relative to the Gondwanan reference site (Fig. 11). Our data set significantly enlarges the information on potential ccw and cw rotations in the Moroccan Meseta showing distinct cw rotations of NL, MEC and the northernmost basins of TID and BOUA, tendencies of ccw rotation of JEB and MTA (although not well resolved due to overlapping uncertainty intervals) and no clear basin-range rotation for CHO, BOUH and KHE in broad agreement with the fold test results shown in Fig. 8. Additionally, relative rotations within basins are also observed (Figs. 11 and 12). Since the stratigraphic position of sampled sites is not well constrained, we cannot ultimately define the timing of rotation of the pull apart basins. Declination values mainly based on Adria data of Channell et al. (2022) are well within rotational uncertainties of the APWP of Africa for using only averaged poles for 260 Ma and 280 Ma derived from a compilation of several separate areas. A recent study based on late Permian rocks from the Argana Basin did not reveal any large scale declination variations (Kent et al., 2021), which is an argument for an age of rotation close to the deposition/emplacement of the sediments/volcanics of the Meseta block. It has to be noted, however, that this conclusion is not final, and more data is needed to ultimately constrain the age of rotational variation within the Meseta block.

Vertical axis rotations are present within and between the pull-apart basins. However, extent and rotational sense is not consistent. For the southern basins of the Jebilet and Rehamna massifs declination deviation seems to increase when going from NE to SW (Fig. 12), which would suggest a continuous rotation of a larger block. In contrast, observed vertical axis rotations of the northern basins of the Central massif follow no structural trend, but rather resemble brittle, fragmented rotations of multiple small blocks (Fig. 12; e.g. Todrani et al., 2020). According to Elter et al. (2020), dextral shearing of Laurasia with respect to Gondwana in the late Paleozoic might have dismembered the northern margin of Gondwana into various "Gondwana derived continental (GDC)" crustal blocks that subsequently suffered differential rotations. Rotational movements between the basins can be explained by the ball-bearing model as proposed by Aubele et al. (2012) consistent with a large shear system between the south and north of Pangea. By sampling

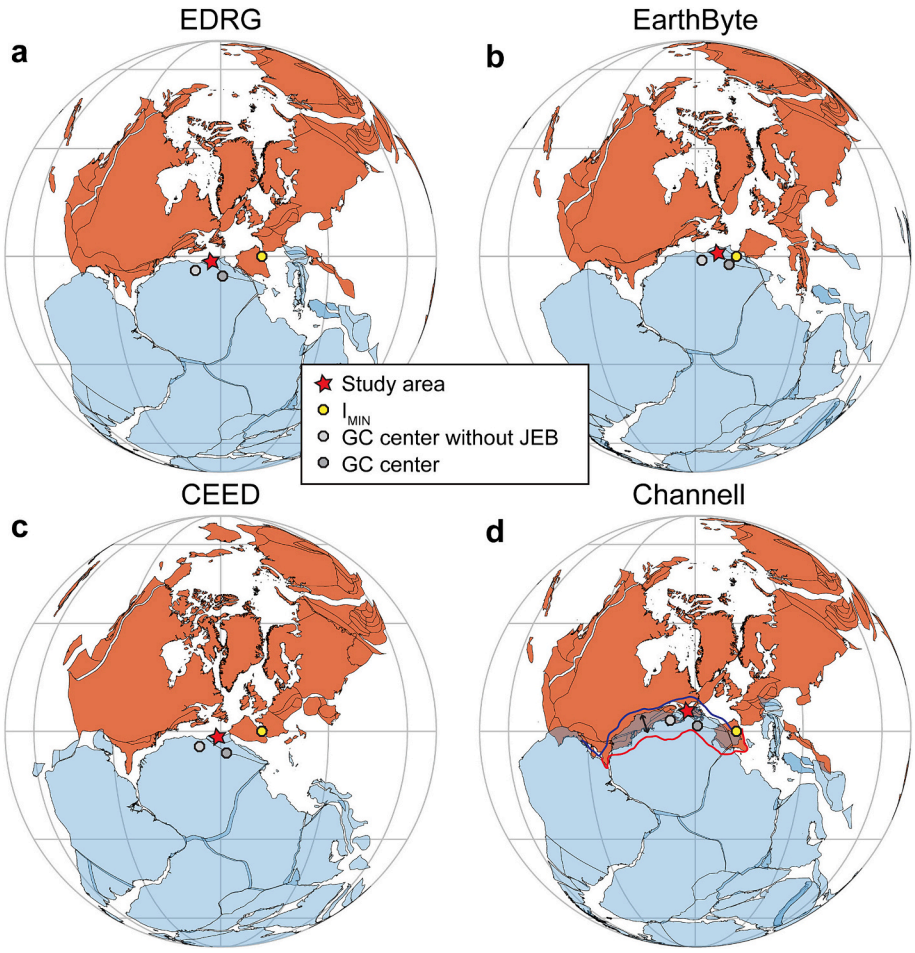

Fig. 13. Paleogeographic reconstructions for 280 Ma, where blue continents correspond to Gondwana and orange ones to Laurussia. Red star indicates the study area in Morocco. (a-d) shows four different reconstructions based on paleogeographic models of: (a): Earth Dynamics Research Group, EDRG: Wu et al. (2024), (b): EarthByte: Merdith et al. (2021), (c): The Centre for Earth Evolution and Dynamics: Torsvik et al. (2014), (d): Channell et al. (2022). Model (d) also shows the reconstructed modern continent ocean boundaries visualizing the resulting continental overlap (Domeier et al., 2021). Also shown are the centers of great circle fits of our ca. 280 Ma data with (dark grey circle) and without paleopole of area JEB (light grey circle) together with the proposed location of I_{MIN} (yellow circle), around which true polar wander should take place (Torsvik et al., 2014). (For interpretation of the references to colour in this figure legend, the reader is referred to the web version of this article.)

the Moroccan Meseta we approached the presumed location of the Pangean mega-shear zone in the Mediterranean from the south and thus might have documented its distal effect on (northern) Moroccan basins.

6. Implications of the Morocco data for Pangea

6.1. Paleolatitudes and plate tectonic reconstructions

Generally, the paleolatitude of the VGPs (site-level) and paleopoles (basin-level) are much more confined spreading only about 20° (Fig. 11). The predicted basin-mean paleolatitudes of this work agree well within uncertainty bonds with previous results of Domeier et al. (2021) for the stable latitudinal position of the Moroccan Meseta (and Northern Africa) in the early Permian and also with reference values based on the APWP of Torsvik et al. (2012). It has to be noted that our data seem to imply a southward motion of the Meseta block between ca. 300 and 275 Ma, which would mean that the Meseta block underwent a disconnected motion compared to Gondwana, which moved rather northward (Fig. 11). However, all our data matches the expected paleolatitude curve of Gondwana within error limits, making any robust statements about potential separate movements of Gondwana and Meseta not statistical viable at this stage.

While the 260 Ma mean paleopole of Channell et al. (2022) coincides well with the reference paleolatitudes, the 280 Ma averaged paleopole shows a notable ~10° difference to the 280 Ma predicted paleolatitude from the Gondwana APWP and also deviating from this study's primary results (Fig. 11). For the calculation of the Cisuralian overall mean paleopole, Channell et al. (2022) mainly adopted the paleomagnetic compilation of Kent and Muttoni (2020) by including seven paleopoles from Adria as a proxy for Gondwana (from a total of 13 paleopoles used, see their Table 2). Pastor-Galán (2022) averaged all Adria poles documented in Kent and Muttoni (2020) into one pole and observed a similar paleolatitude deviation from the global apparent polar wander path rotated into Gondwana coordinates (their Fig. 5). Therefore, inclusion or exclusion of paleomagnetic data from Adria is the key difference leading to presence or absence of the latitudinal overlap of Gondwana and Laurasia. Hence in contrast to our results on declinational variations, the paleolatitudinal results do not reinforce the validity of Pangea B. It should be pointed out that a late Carboniferous to earliest Permian Pangea B configuration as proposed by Klootwijk (2023) cannot be addressed using our dataset because the earlier data is not as numerous and robust (Fig. 11). Another problem regarding this time interval is related to a general spread of paleomagnetic data during the early Permian (Wu et al., 2015). Accordingly, more studies with a high site number like ours should be carried out for more places of Gondwana and Laurussia to complete our paleogeographic understanding of the

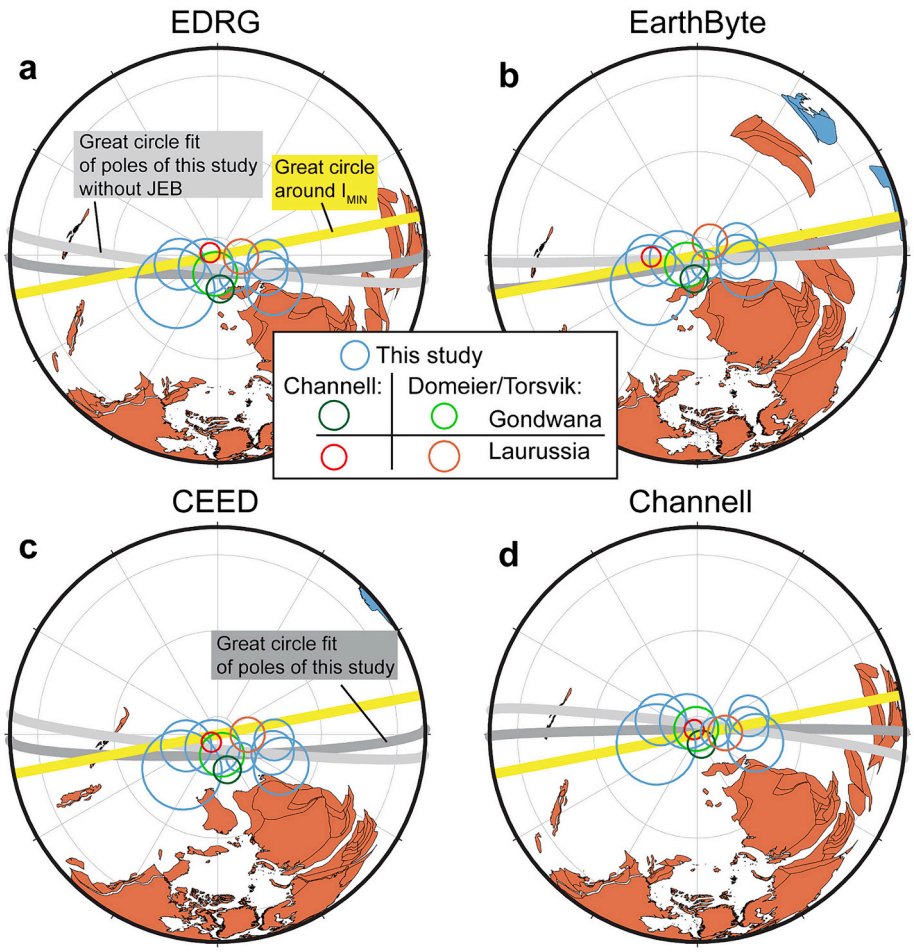

Fig. 14. Reconstructed paleopoles according to reconstructions of Fig. 13 from Gondwana: light green: Domeier et al. (2021), dark green: Channell et al. (2022) and Laurussia: orange:, Torsvik et al. (2012), red: Channell et al. (2022) together with our coeval results (blue) of ca. 280 Ma from the Moroccan Meseta block (see Table 2 for details). Also shown are great circles around the proposed I_{MIN} of this time (Torsvik et al., 2014) in yellow and fits to our data in light grey (our data of ca. 280 Ma without paleopole of area JEB) and dark grey (all our data of ca. 280 Ma). (For interpretation of the references to colour in this figure legend, the reader is referred to the web version of this article.)

assembly of Pangea.

To assess the implications of our data from the Meseta block for global reconstructions during the Permian we follow the approach of Domeier et al. (2021). Accordingly, we plot the paleopoles for Laurussia without inclination shallowing correction at 280 Ma (Torsvik et al., 2012) and the modified paleopoles for Gondwana for the same age (GP2 of Domeier et al., 2021). Our colouring of Gondwana (blue) and Laurussia (red) follows figure 16 of Domeier et al. (2021). Additionally, we plot a great circle fit to our data of ca. 280 Ma with and without the slightly younger area of JEB. The centers of the great circle fits are very close to the actual sampling locality. As expected from Fig. 11, in terms of paleolatitudes our new extensive Gondwana-related dataset is in agreement with all three major continental reconstructions of Gondwana and Laurussia without a significant overlap at ca. 280 Ma (Fig. 13). There is a spread of our paleopoles visible, which does not seem to be correlated to an age progression (Figs. 10, 11, 14). As discussed earlier, this spread can be explained by vertical axis rotations affecting the various basins with different amplitudes resembling late Paleozoic rotation patterns in SE France (Aubele et al., 2012) and Sardinia (Aubele et al., 2014; Bachtadse et al., 2018; Siravo et al., 2023). It is interesting to note that a great circle around the proposed minimum-inertial axis (I_{MIN}) also seem to fit our paleopole data (Fig. 14). A true polar wander (TPW) related explanation appears possible based on the sense of spread, especially when taking into account that the sampling locality is located very close to I_{MIN} (Fig. 13), which could lead to rapid declination variations. More data is needed to further address this possibility.

6.2. *Moroccan data in a global context*

To put our paleomagnetic results in a global context, we focus on the implications for a 280 Ma time, which is the crucial age when a significant overlap between Gondwana and Laurussia was identified (Channell et al., 2022). We show three continental reconstruction models (Fig. 13) : Earth Dynamics Research Group (Wu et al., 2024), Earthbyte (Merdith et al., 2021), CEED (Torsvik et al., 2014) and a model constructed using Gondwana and Laurussia poles based on Channell et al. (2022). Fig. 14 shows the resulting paleopoles from Gondwana (based on Domeier et al. (2021) and Channell et al. (2022)), Laurussia (based on Torsvik et al. (2012) and Channell et al. (2022)) and from Morocco (this study) in each paleogeographic reconstruction. It has to be noted that Channell et al. (2022) did include Moroccan data from the Meseta block of Domeier et al. (2021) in their 280 Ma mean paleopole of Gondwana as well as data from Adria. Inspection of Figs. 13 and 14 reveals that our Meseta data is in general agreement of all presented paleogeographic models, where our data seems to be better represented by the Gondwana mean pole of Domeier et al. (2021), rather than that by Channell et al. (2022). Ultimately, since our data are also compatible with the Channell et al. (2022) reconstruction, the presence or absence of the latitudinal overlap of Gondwana and Laurussia is related to the small confidence intervals of Channell et al. (2022)'s paleopoles and the

inclusion of the Adria data, which slightly moves the Gondwana mean pole (Fig. 14). In summary, the Meseta paleomagnetic data do not support a large latitudinal overlap of Gondwana and Laurussia and does therefore not require a Pangea B configuration in the early Permian. Our results stress again the importance of the structural relationship of Adria and Gondwana as the key to resolve the Pangea controversy.

7. Conclusions

The presented paleomagnetic collection from Morocco represents one of the biggest entries in the paleomagnetic data base for the Late Paleozoic of the recent past. By integrating age constraints derived from recent radiometric dating, stratigraphy and paleontology we could further resolve and update the tectonic and paleogeographic setting for NW Africa (resp. Gondwana) provided by Domeier et al. (2021).

Apart from a late Permian remagnetization of the southernmost basin of ZAT revealed by negative fold tests, at least one type of fold test shows a positive outcome for all remaining basins. Matching paleolatitudes for the respective age models and presence of reversals at three basins (MTA, CHO and BOUH) that could be correlated to the late-Artinskian CI2n normal magnetochron (281.24 ± 2.3 Ma) within the Kiaman reversed superchron support a primary character of the latter.

The VGPs are elongated in a NE-SW sense and strung out along a small circle band intersecting the early Permian portion of the APWP of Gondwana with the Euler pole located within the study area thus showing CW and – to a minor extent – CCW vertical axis rotations on site and basin level. Since observed paleolatitudes are located close to the paleoequator and no striking difference between the volcanic and red bed samples was observed, inclination shallowing has not altered the paleomagnetic signal.

Since paleomagnetic data from Adria has repeatedly been used to extend the sparse available data set for Gondwana and has been invoked as supportive evidence for the validity of Pangea B, we compared a 280 Ma mean paleopole that combined all available early Permian information of Gondwana and Adria (Channell et al., 2022) with our results derived directly from Gondwana. The paleolatitude determined from the combined pole is within error of the newly obtained data, but slightly offset towards higher values. We used our paleopole data in the most up-to-date continental paleogeographic reconstructions to investigate the significance of the Moroccan data in the ongoing Pangea debate. Our data confirms previous data by Domeier et al. (2021) and overlaps with Gondwanan mean poles by Domeier et al. (2021) and by Channell et al. (2022). Accordingly, our data does not require a large continental overlap and therefore a Pangea B configuration, but it also stresses that ultimately only the inclusion/exclusion of paleomagnetic data from Adria can resolve the Pangea controversy. The potential vertical axis rotations within the Meseta block can be interpreted as additional support to the existence of a major intra Pangea shear zone as proposed by Aubele et al. (2014).

Declaration of competing interest

The authors declare the following financial interests/personal relationships which may be considered as potential competing interests:

Vinzenz Weissbrodt, Valerian Bachtadse reports financial support was provided by German Research Foundation.

Data availability

Data will be made available on request.

Acknowledgements

VB, VW and AR were supported by the German Research Council (DFG) Grant Ba1210/24-1 awared to VB. We are thankful to Giovanni Muttoni who triggered the project and who commented on earlier drafts of the manuscript. UK acknowledges funding from an Australian Research Council Discovery Project (DP210102495) awarded to Zheng-Xiang Li and Andy J Biggin. AR acknowledges PRIN Project n.2022ZH5RWP DEtailing thE Paleogeography of Southern PAlaeoeurope by meanS of biosTratigraphic correlation and basin development in the Paleozoic to early Mesozoic time-frame: case histories from the Italian record (DEEP PAST).

Appendix A. Supplementary data

Supplementary data to this article can be found online at https://doi.org/10.1016/j.earscirev.2024.104787.

References

Aassoumi, H., Vozenin-Serra, C., 1996. Sur un bois silicifie a moelle conservee du Permien du Bassin de Tiddas (Maroc Central), Mesopityoxylon tiddasense gen. et sp. nov. – Interets phylogenetique et paleoclimatique. Rev. Palaeobot. Palynol. 1 (94), 57–73.

Aassoumi, H., Broutin, J., Youbi, N., El Wartiti, M., Galtier, J., 1992. Découverte de Scleromedulloxylon Cf. Aveyronense, Bois Fossile de coniférophyte Dans le Complexe Volcanique Permien du Bassin de Khenifra (Maroc Central). OFP Informations.

Aretz, M., Herbig, H.-G., Wang, X., Gradstein, F., Agterberg, F., Ogg, J., 2020. The carboniferous period. In: Geologic Time Scale 2020. Elsevier, pp. 811–874.

Arthaud, F., Matte, P., 1977. Late Paleozoic strike-slip faulting in southern Europe and northern Africa: result of a right-lateral shear zone between the Appalachians and the Urals. Geol. Soc. Am. Bull. 88 (9), 1305–1320.

Aubele, K., Bachtadse, V., Muttoni, G., Ronchi, A., Durand, M., 2012. A paleomagnetic study of Permian and Triassic rocks from the Toulon-Cuers Basin, SE France: evidence for intra-Pangea block rotations in the Permian. Tectonics 31 (3), TC3015.

Aubele, K., Bachtadse, V., Muttoni, G., Ronchi, A., 2014. Paleomagnetic data from late Paleozoic dykes of Sardinia: evidence for block rotations and implications for the intra-Pangea megashear system. Geochem. Geophys. Geosyst. 15 (5), 1684–1697.

Bachtadse, V., Aubele, K., Muttoni, G., Ronchi, A., Kirscher, U., Kent, D.V., 2018. New early Permian paleopoles from Sardinia confirm intra-Pangea mobility. Tectonophysics 749, 21–34.

Barbero, L., Jabaloy, A., Gomez-Ortiz, D., Perez-Pena, J.V., Rodriguez-Peces, M.J., Tejero, R., Estupinan, J., Azdimousa, A., Vazquez, M., Asebriy, L., 2011. Evidence for surface uplift of the Atlas Mountains and the surrounding peripheral Plateaux: Combining apatite fission-track results and geomorphic indicators in the Western Moroccan Meseta (coastal Variscan Paleozoic basement). Tectonophysics 502 (1–2), 90–104.

Becker, T.P., Thomas, W.A., Samson, S.D., Gehrels, G.E., 2005. Detrital zircon evidence of Laurentian crustal dominance in the lower Pennsylvanian deposits of the Alleghanian clastic wedge in eastern North America. Sediment. Geol. 182 (1–4), 59–86.

Boutsougame, A., Ouazzani, H., El Hadi, H., Eddif, A., 2016. Volcanisme Permien Du Massif De Chougrane-El had Des Bouhsoussène (Maroc Central, Maroc). Eur. Sci. J. 12 (27), 81–92.

Broutin, J., Aassoumi, H., El Wartiti, M., Freytet, P., Kerp, H., 1998. The Permian basins of Tiddas, Bou Achouch and Khenifra (Central Morocco). Biostratigraphic and palaeophytogeographic implications. Mémoires du Muséum national d'histoire naturelle (1993) 179, 257–278.

Cailleux, Y., Gonord, H., Le Guern, M., Sauvage, M., 1983. Taphrogenèse et magmatisme permien dans le Maroc central. Bull. Fac. Sci. Marrakech 1 (1), 24–39.

Channell, J.E.T., Muttoni, G., Kent, D.V., 2022. Adria in Mediterranean paleogeography, the origin of the Ionian Sea, and Permo-Triassic configurations of Pangea. Earth Sci. Rev. 230, 104045.

Charif, A., Ribeiro, M.L., Ferreira, P., Moreira, E., Ezzouhairi, H., Ait Ayad, N., 1998. Pétrogenèse Des Vulcanites autuniènnes de Nzalt-Laracha Des Rehamna Orientaux. Méséta centrale, Maroc.

Chopin, F., Corsini, M., Schulmann, K., El Houicha, M., Ghienne, J.F., Edel, J.B., 2014. Tectonic evolution of the Rehamna metamorphic dome (Morocco) in the context of the Alleghanian-Variscan orogeny. Tectonics 33 (6), 1154–1177.

Daly, L., Pozzi, J.P., 1976. Resultats paleomagnetiques du Permien inferieur et du Trias marocain; comparaison avec les donnees africaines et Sud americaines. Earth Planet. Sci. Lett. 29, 71–80.

Damotte, R., El Wartiti, M., Freytet, P., Khounch, H., Lethiers, F., Totin-Morin, N., 1993. Le bassin de Mechraa Ben Abbou (Rehamna, maroc): son insertion dans le contexte permien du Maroc central et mésétien. In: 118ème Congr. nat. Soc. hist. scient., 4ème Colloque Géologie africaine, Bassins sédimentaires africains, Paris (ed. Comité Trav. Hist. Scientif.), pp. 53–72.

Delchini, S., Lahfid, A., Plunder, A., Michard, A., 2016. Applicability of the RSCM geothermometry approach in a complex tectono-metamorphic context: the Jebilet massif case study (Variscan Belt, Morocco). Lithos 256, 1–12.

Delchini, S., Lahfid, A., Lacroix, B., Baudin, T., Hoepffner, C., Guerrot, C., Lach, P., Saddiqi, O., Ramboz, C., 2018. The Geological Evolution of the Variscan Jebilet Massif, Morocco, Inferred from New Structural and Geochronological analyses. Tectonics 37 (12), 4470–4493.

Doblas, M., Oyarzun, R., Lopez-Ruiz, J., Cebria, J.M., Youbi, N., Mahecha, V., Lago, M., Pocovi, A., Cabanis, B., 1998. Permo-Carboniferous volcanism in Europe and

Northwest Africa: a superplume exhaust valve in the Centre of Pangaea? J. Afr. Earth Sci. 26 (1), 89–99.
Domeier, M., Van der Voo, R., Torsvik, T.H., 2012. Paleomagnetism and Pangea: the road to reconciliation. Tectonophysics 514, 14–43.
Domeier, M., Font, E., Youbi, N., Davies, J., Nemkin, S., Van der Voo, R., Perrot, M., Benabbou, M., Boumehdi, M.A., Torsvik, T.H., 2021. On the early Permian shape of Pangea from paleomagnetism at its core. Gondwana Res. 90, 171–198.
Doubinger, J., Roy-Dias, C., 1985. La paléoflore du Stéphanien de l'Oued zat (Haut-Atlas de Marrakech—versant nord—Maroc). Geobios 18 (5), 573–593.
Edel, J.B., Schulmann, K., Lexa, O., Lardeaux, J.M., 2018. Late Palaeozoic palaeomagnetic and tectonic constraints for amalgamation of Pangea supercontinent in the European Variscan belt. Earth Sci. Rev. 177, 589–612.
El Hadi, H., Tahiri, A., El Maidani, A., Saddiqi, O., Simancas, F., González Lodeiro, F., Azor, A., Martinez-Poyatos, D., Tahiri, M., De La Rosa Diaz, J., 2014. Geodynamic Setting Context of the Permian and Triassic Volcanism in the Northwestern Moroccan Meseta from Petrographical and Geochemical Data.
El Kamel, F., 1987. Géologie du paléozoïque Des Rehamna Nord-Orientaux, Maroc. Évolution sédimentaire et structuration hercynienne d'un bassin dévono-carbonifère. Sédimentation et déformation des molasses post-orogénique. Université Paul Cézanne-Aix-Marseille III.
El Wartiti, M., 1981. Les Terrains Permo-Carbonifères et Leur Couverture dans la Zone de Tiddas-Souk es Sebt (Bordure Nord-Ouest de la Méséta Marocaine. Nord du Maroc Central). Mohamed V Rabat, Morocco, 193 pp.
El Wartiti, M., 1996. Synthèse sur le Permien du Maroc. In: Medina, F. (Ed.), Le Permien et le Trias du Maroc: état des connaissances, pp. 1–17. Editions PUMAG.
El Wartiti, M., Broutin, J., Freytet, P., 1986. Premières découvertes paléontologiques dans les séries rouges carbonatées permiennes du bassin de Tiddas (Maroc Central). Comptes rendus de l'Académie des sciences. Série 2, Mécanique, Physique, Chimie, Sciences de l'univers. Sci. Terre 303 (3), 263–268.
El Wartiti, M.E., Broutin, J., Freytet, P., Larhrib, M., Toutin-Morin, N., 1990. Continental deposits in Permian basins of the Mesetian Morocco, geodynamic history. J. Afr. Earth Sci. 10 (1–2), 361–368.
El Wartiti, M., Jebrak, M., Cabanis, B., Toutin-Morin, N., Youbi, N., 1992. 7ès Journèe Thèmatiques de l'Assoc. Geol. Permien Paris des rèsumes, 7.
Elter, F.M., Gaggero, L., Mantovani, F., Pandeli, E., Costamagna, L.G., 2020. The Atlas-East Variscan -Elbe shear system and its role in the formation of the pull-apart late Palaeozoic basins. Int. J. Earth Sci. 109 (3), 739–760.
Enkin, R.J., Watson, G.S., 1996. Statistical analysis of palaeomagnetic inclination data. Geophys. J. Int. 126, 495–504.
Essaifi, A., Hibti, M., 2008. The hydrothermal system of Central Jebilet (Variscan Belt, Morocco): a genetic association between bimodal plutonism and massive sulphide deposits? J. Afr. Earth Sci. 50 (2–4), 188–203.
Evans, M., Pavlov, V., Veselovsky, R., Fetisova, A., 2014. Late Permian paleomagnetic results from the Lodève, Le Luc, and Bas-Argens Basins (southern France): Magnetostratigraphy and geomagnetic field morphology. Phys. Earth Planet. Inter. 237, 18–24.
Fisher, R., 1953. Dispersion on a sphere. Proc. R. Soc. Lond. A Math. Phys. Eng. Sci. 217 (1130), 295–305.
Fisher, N.I., Lewis, T., Embleton, B.J., 1993. Statistical Analysis of Spherical Data. Cambridge university press.
Fluteau, F., Besse, J., Broutin, J., Ramstein, G., 2001. The late Permian climate. What can be inferred from climate modelling concerning Pangea scenarios and Hercynian range altitude? Palaeogeogr. Palaeoclimatol. Palaeoecol. 167 (1–2), 39–71.
Foner, S., 1959. Versatile and sensitive vibrating-sample magnetometer. Rev. Sci. Instrum. 30, 548–557.
Gigout, M., 1951. Etudes géologiques Sur la Méséta marocaine occidentale (arrière-pays de Casablanca, Mazagan et Safi). In: Notes et Mèmoires du Service-Géologique du Maroc, 86. Rabat, Maroc Matin.
Gordon, R.G., 1998. The plate tectonic approximation: plate nonrigidity, diffuse plate boundaries, and global plate reconstructions. Annu. Rev. Earth Planet. Sci. 26 (1), 615–642.
Gradstein, F.M., Ogg, J.G., Schmitz, M.D., Ogg, G.M., 2020. Geologic Time Scale 2020. Elsevier.
Guiraud, R., Bosworth, W., Thierry, J., Delplanque, A., 2005. Phanerozoic geological evolution of Northern and Central Africa: an overview. J. Afr. Earth Sci. 43 (1–3), 83–143.
Hadimi, I., Ait Lahna, A., Assafar, H., Tassinari, C.C.G., Youbi, N., Boumehdi, M.A., Bensalah, M.K., Gaggero, L., Mata, J., Doblas, M., Basei, M.A.S., Sato, K., L, R.M., Charif, A., El Aarab, M., Ben Abbou, M., Zouita, F., Khounch, H., 2018. The Post-Collisional Hercynian Volcanism of Rehamna, Western Meseta, Morocco. In: Mineral Chemistry, Petrology and U-Pb dating. 2eme Congres International sur le Permien et le Trias, Casablanca 25-27 aprile, 2018, Abstract book.
Hadimi, I., Youbi, N., Lahna, A.A., Bensalah, M.K., Moutbir, O., Mata, J., Doblas, M., Tassinari, C.C.G., Gaggero, L., Basei, M.A.S., Sato, K., El Moume, W., Boumehdi, M. A., 2021. U-Pb Zircon Geochronological and Petrologic Constraints on the Post-Collisional Variscan Volcanism of the Tiddas-Souk Es-Sebt des Ait Ikko Basin (Western Meseta, Morocco). Minerals 11 (10).
Henderson, C., Shen, S., Gradstein, F., Agterberg, F., 2020. The permian period. In: Geologic Time Scale 2020. Elsevier, pp. 875–902.
Hmich, D., Schneider, J., Saber, H., Voigt, S., El Wartiti, M., 2006. New continental Carboniferous and Permian faunas of Morocco: implications for biostratigraphy, palaeobiogeography and palaeoclimate. Geol. Soc. Lond. Spec. Publ. 265 (1), 297–324.
Hoepffner, C., 1982. Le magmatisme pré-et post-orogénique hercynien dans le Paléozoïque des Rehamna. Notes Serv. Géol. Maroc 303, 150–163.
Hoepffner, C., Soulaimani, A., Pique, A., 2005. The Moroccan Hercynides. J. Afr. Earth Sci. 43 (1–3), 144–165.
Hoepffner, C., Houari, M.R., Bouabdelli, M., 2006. Tectonics of the North African variscides (Morocco, Western Algeria): an outline. Compt. Rendus Geosci. 338 (1–2), 25–40.
Hounslow, M., 2006. PMagTools version 4.2-a tool for analysis of 2-D and 3-D directional data.
Hounslow, M.W., 2022. A geomagnetic polarity timescale for the Carboniferous. Geol. Soc. Lond. Spec. Publ. 512 (1), 141–195.
Hounslow, M.W., Balabanov, Y.P., 2018. A geomagnetic polarity timescale for the Permian, calibrated to stage boundaries. In: Lucas, S.G., Shen, S.Z. (Eds.), Permian Timescale. Geological Society Special Publication, pp. 61–103.
Huvelin, P., 1977. Etude Geologique et Gitologique Du Massif Hercynien Des Jebilet (Maroc Occidental). In: Notes et Mèmoires du Sérvice Gèologique du Maroc, 232 bis: 307 pp.
Irving, E., 1977. Drift of Major Continental Blocks since Devonian. Nature 270 (5635), 304–309.
Irving, E., 2013. The Case for Pangea B, and the Intra-Pangean Megashear. In: Channell, J.E.T., Kent, D.V., Lowrie, W., Meert, J.G. (Eds.), Geophysical Monograph Series. American Geophysical Union, Washington, D. C, pp. 13–27.
Irving, E., Morel, P., 1978. Paleozoic continental-drift. Trans. Am. Geophys. Union 59 (4), 263.
Jebrak, M., 1985. Contribution a l'histoire Naturelle Des Filons(F, Ba) du Domaine Varisque Francais et Marocain: Essai de Caracterisation Structurale et Geochimique Des Filons en Extension et en Decrochement. Universite d'Orleans.
Kent, D.V., Muttoni, G., 2020. Pangea B and the late Paleozoic ice age. Palaeogeogr. Palaeoclimatol. Palaeoecol. 553, 109753.
Kent, D.V., Olsen, P.E., Muttoni, G., Et-Touhami, M., 2021. A late Permian paleopole from the Ikakern Formation (Argana basin, Morocco) and the configuration of Pangea. Gondwana Res. 92, 266–278.
Kerp, H., Broutin, J., Lausberg, S., Aassoumi, H., 2001. Discovery of latest Carboniferous–Early Permian radially symmetrical peltaspermaceous megasporophylls from Europe and North Africa. Compt. Rend. l'Acad. Sci. Ser. IIA-Earth Planet. Sci. 332 (8), 513–519.
King, R., 1955. The remanent magnetism of artificially deposited sediments. Geophys. Suppl. Monthly Notices R. Astron. Soc. 7 (3), 115–134.
Kirscher, U., Aubele, K., Muttoni, G., Ronchi, A., Bachtadse, V., 2011. Paleomagnetism of Jurassic carbonate rocks from Sardinia: no indication of post-Jurassic internal block rotations. J. Geophys. Res. Solid Earth 116.
Kirscher, U., Bilardello, D., Mikolaichuk, A., Bachtadse, V., 2014. Correcting for inclination shallowing of early Carboniferous sedimentary rocks from Kyrgyzstan-indication of stable subtropical position of the North Tianshan Zone in the mid-late Palaeozoic. Geophys. J. Int. 198 (2), 1000–1015.
Kirschvink, J.L., 1980. The least-squares line and plane and the analysis of palaeomagnetic data. Geophys. J. R. Astron. Soc. 62 (3), 699–718.
Klootwijk, C., 2023. Matching mid-to-latest Carboniferous pole path segments for eastern Australia and northern Armorica indicate a late Carboniferous Pangea-B configuration and a mid Carboniferous inertial interchange true polar wander event. Earth Sci. Rev. 104521.
Kodama, K.P., 2012. Paleomagnetism of Sedimentary Rocks: Process and Interpretation. John Wiley & Sons.
Koymans, M.R., Langereis, C.G., Pastor-Galán, D., van Hinsbergen, D.J.J., 2016. Paleomagnetism.org: an online multi-platform open source environment for paleomagnetic data analysis.
Koymans, M., van Hinsbergen, D., Pastor-Galán, D., Vaes, B., Langereis, C., 2020. Towards FAIR paleomagnetic data management through Paleomagnetism. org 2.0. Geochem. Geophys. Geosyst. 21 (2), e2019GC008838.
Krása, D., Petersen, K., Petersen, N., 2007. In: Gubbins, D., Herrero-Bervera, E. (Eds.), Variable field translation balance. Springer, Dordrecht, The Netherlands, pp. 97–99.
Lanari, R., Faccenna, C., Fellin, M.G., Essaifi, A., Nahid, A., Medina, F., Youbi, N., 2020. Tectonic evolution of the Western High Atlas of Morocco: oblique convergence, reactivation, and transpression. Tectonics 39 (3).
Larhrib, M., 1988. Les Formations Permiennes et Triasico-Mio-Quaternaires des Régions de Tiddas. In: Maaziz et Sebt Aït Ikko (NW du Maroc Central). Stratigraphie, Sédimentologie et Reconstitution Des Paléoenvironnements Sédimentaires, Ecole Normale Supérieure Rabat, Morocco, Rabat.
Larhrib, M., 1996. Flore Fossile et séquences Des Formations Rouges Fluviatiles du Bassin Autunien de Tiddas-Sebt Aït Ikkou (Nord-Ouest du Maroc Central), Le Permien et le Trias du Maroc: état Des Connaissances. Presses Universitaires du Maghreb, Marrakech, pp. 19–29.
Martin, D.L., Nairn, A.E.M., Noltimier, H.C., Petty, M.H., Schmitt, T., 1978. Palaeozoic and Mesozoic palaeomagnetic results from Morocco. Tectonophysics 44, 91–114.
Merdith, A.S., Williams, S.E., Collins, A.S., Tetley, M.G., Mulder, J.A., Blades, M.L., Young, A., Armistead, S.E., Cannon, J., Zahirovic, S., 2021. Extending full-plate tectonic models into deep time: linking the Neoproterozoic and the Phanerozoic. Earth Sci. Rev. 214, 103477.
Michard, A., 1976. Eléments de Géologie marocaine. Notes Mèm. Sérv. Gèol. Maroc 252, 408 pp.
Michard, A., 1982. Le massif paléozoïque des Rehamna (Maroc) stratigraphie, tectonique et petrogenese d'un segment de la chaine varisque. Notes Mèm. Sérv. Gèol. Maroc 303, 108p.
Michard, A., Saddiqi, O., Chalouan, A., de Lamotte, D.F., 2008. Continental Evolution: The Geology of Morocco: Structure, Stratigraphy, and Tectonics of the Africa-Atlantic-Mediterranean Triple Junction. Springer, Berlin Heidelberg.
Michard, A., Ouanaimi, H., Hoepffner, C., Soulaimani, A., Baidder, L., 2010a. Comment on Tectonic relationships of Southwest Iberia with the allochthons of Northwest

Iberia and the Moroccan Variscides by JF Simancas et al. C. R. Geoscience 341 (2009) 103-113. Compt. Rendus Geosci. 342 (2), 170–174.
Michard, A., Soulaimani, A., Hoepffner, C., Ouanaimi, H., Baidder, L., Rjimati, E.C., Saddiqi, O., 2010b. The South-Western Branch of the Variscan Belt: evidence from Morocco. Tectonophysics 492 (1–4), 1–24.
Mitchell, R.N., Zhang, N., Salminen, J., Liu, Y., Spencer, C.J., Steinberger, B., Murphy, J. B., Li, Z.-X., 2021. The supercontinent cycle. Nat. Rev. Earth Environ. 2 (5), 358–374.
Morel, P., Irving, E., 1981. Paleomagnetism and the Evolution of Pangea. J. Geophys. Res. 86 (Nb3), 1858–1872.
Morel, P., Irving, E., Daly, L., Moussinepouchkine, A., 1981. Paleomagnetic results from Permian Rocks of the Northern Saharan Craton and Motions of the Moroccan Meseta and Pangea. Earth Planet. Sci. Lett. 55 (1), 65–74.
Müller, R.D., Cannon, J., Qin, X., Watson, R.J., Gurnis, M., Williams, S., Pfaffelmoser, T., Seton, M., Russell, S.H., Zahirovic, S., 2018. GPlates: building a virtual Earth through deep time. Geochem. Geophys. Geosyst. 19 (7), 2243–2261.
Muttoni, G., Kent, D.V., 2019. Adria as promontory of Africa and its conceptual role in the Tethys twist and Pangea B to Pangea A transformation in the Permian. Riv. Ital. Paleontol. Stratigr. 125 (1), 249–269.
Muttoni, G., Kent, D.V., Garzanti, E., Brack, P., Abrahamsen, N., Gaetani, M., 2003. Early Permian Pangea 'B' to Late Permian Pangea 'A'. Earth Planet. Sci. Lett. 215 (3–4), 379–394.
Muttoni, G., Gaetani, M., Kent, D.V., Sciunnach, D., Angiolini, L., Berra, F., Garzanti, E., Mattei, M., Zanchi, A., 2009. Opening of the neo-Tethys Ocean and the Pangea B to Pangea A transformation during the Permian. GeoArabia (Manama) 14 (4), 17–48.
Muttoni, G., Dallanave, E., Channell, J.E.T., 2013. The drift history of Adria and Africa from 280 Ma to present, Jurassic true polar wander, and zonal climate control on Tethyan sedimentary facies. Palaeogeogr. Palaeoclimatol. Palaeoecol. 386, 415–435.
Pastor-Galán, D., 2022. From supercontinent to superplate: late Paleozoic Pangea's inner deformation suggests it was a short-lived superplate. Earth Sci. Rev. 226, 103918.
Perez, N.D., Teixell, A., Gomez-Gras, D., Stockli, D.F., 2019. Reconstructing Extensional Basin Architecture and Provenance in the Marrakech High Atlas of Morocco: Implications for Rift Basins and Inversion Tectonics. Tectonics 38 (5), 1584–1608.
Pohl, F., Froitzheim, N., Obermüller, G., Tomaschek, F., Schröder, O., Nagel, T.J., Sciunnach, D., Heuser, A., 2018. Kinematics and age of syn-intrusive detachment faulting in the Southern Alps: evidence for early Permian crustal extension and implications for the Pangea a versus B Controversy. Tectonics 37 (10), 3668–3689.
Rochette, P., Vandamme, D., 2001. Pangea B: An Artifact of Incorrect Paleomagnetic Assumptions?.
Saber, H., El Wartiti, M., 1996. Late Hercynian sediment and tectonic history of the Oued Zat and Ida Ou Zal basins (western high Atlas, Morocco) - Transtensive strike-slip basins. J. Afr. Earth Sci. 22 (3), 301–309.
Saber, H., El Wartiti, M., Hmich, D., Schneider, J.W., 2007. Tectonic evolution from the Hercynian shortening to the Triassic extension in the Paleozoic sediments of the Western High Atlas (Morocco). J. Iber. Geol. 33 (1), 31–40.
Saber, H., Hminna, A., Jouhari, A., Rmich, A., 2014. Lithostratigraphy and evidence of an extensive tectonic of lower Permian age in the continental deposits of M'tal (Western Rehamna, Morocco). Am. Int. J. Res. Form. Appl. Nat. Sci. 7, 81–87.
Saddiqi, O., El Haimer, F.Z., Michard, A., Barbarand, J., Ruiz, G.M.H., Mansour, E.M., Leturmy, P., de Lamotte, D., 2009. Apatite fission-track analyses on basement granites from south-western Meseta, Morocco: Paleogeographic implications and interpretation of AFT age discrepancies. Tectonophysics 475 (1), 29–37.
Saidi, A., Tahiri, A., Brahim, L.A., Saidi, M., 2002. Etats de contraintes et mécanismes d'ouverture et de fermeture des bassins permiens du Maroc hercynien. L'exemple des bassins des Jebilet et des Rehamna. Compt. Rend. Géosci. 334 (3), 221–226.
Silantiev, V., Marchetti, L., Ronchi, A., Schirolli, P., Scholze, F., Urazaeva, M., 2022. Permian non-marine bivalves from the Collio and GunCina formations (southern alPs, Italy): revised biostratiGraPhy and PalaeobioGeoGraPhy. Riv. Ital. Paleontol. Stratigr. 128 (1).
Siravo, G., Speranza, F., Mattei, M., 2023. Paleomagnetic evidence for pre-21 Ma independent drift of South Sardinia from North Sardinia-Corsica:"Greater Iberia" vs. Europe. Tectonics e2022TC007705.
Skikra, H., Amrouch, K., Soulaimani, A., Leprêtre, R., Ouabid, M., Bodinier, J.-L., 2021. The intracontinental High Atlas belt: geological overview and pending questions. Arab. J. Geosci. 14 (12), 1071.
Tauxe, L., 2005. Inclination flattening and the geocentric axial dipole hypothesis. Earth Planet. Sci. Lett. 233 (3–4), 247–261.
Tauxe, L., Badgley, C., 1984. Transition stratigraphy and the problem of remanence lock-in times in the Siwalik red beds. Geophys. Res. Lett. 11 (6), 611–613.
Tauxe, L., Kent, D.V., 2004. A simplified statistical model for the geomagnetic field and the detection of shallow bias in paleomagnetic inclinations: was the ancient magnetic field dipolar? Timesc. Paleomagn. Field 145, 101–115.
Tauxe, L., Watson, G.S., 1994. The fold test: an eigen analysis approach. Earth Planet. Sci. Lett. 122, 331–341.
Termier, H., 1936. Etudes géologiques sur le Maroc central et le moyen-Atlas septentrional. Notes et Mém. Serv. Mines et cartes géologiques. Maroc, n° 33, tome IX.
Todrani, A., Zhang, B., Speranza, F., Chen, S., 2020. Paleomagnetism of the middle Cenozoic Mula Basin (East Tibet): evidence for km-scale crustal blocks rotated by midlower crust drag. Geochem. Geophys. Geosyst. 21 (9), e2020GC009225.
Torcq, F., Besse, J., Vaslet, D., Marcoux, J., Ricou, L.E., Halawani, M., Basahel, M., 1997. Paleomagnetic results from Saudi Arabia and the Permo-Triassic Pangea configuration. Earth Planet. Sci. Lett. 148 (3), 553–567.
Torsvik, T.H., Van Der Voo, R., Preeden, U., Mac Niocaill, C., Steinberger, B., Doubrovine, P.V., Van Hinsbergen, D.J.J., Domeier, M., Gaina, C., Tohver, E., Meert, J.G., McCausland, P.J.A., Cocks, L.R.M., 2012. Phanerozoic polar wander, palaeogeography and dynamics. Earth Sci. Rev. 114 (3–4), 325–368.
Torsvik, T.H., Van Der Voo, R., Doubrovine, P.V., Burke, K., Steinberger, B., Ashwal, L.D., Trønnes, R.G., Webb, S.J., Bull, A.L., 2014. Deep mantle structure as a reference frame for movements in and on the Earth. Proc. Natl. Acad. Sci. 111 (24), 8735–8740.
Torsvik, T., Smethurst, M., Pesonen, L., 2015. GMAP. Geographic Mapping and Palaeoreconstruction Package. Norwegian Geological Survey Report, p. 90.
Vai, G.B., 2003. Development of the palaeogeography of Pangaea from late Carboniferous to early Permian. Palaeogeogr. Palaeoclimatol. Palaeoecol. 196 (1–2), 125–155.
Van der Voo, R., 1990. The reliability of paleomagnetic data. Tectonophysics 184, 1–9.
Van der Voo, R., Torsvik, T.H., 2001. Evidence for late Paleozoic and Mesozoic nondipole fields provides an explanation for the Pangea reconstruction problems. Earth Planet. Sci. Lett. 187, 71–81.
Van Hilten, D., 1964. Evaluation of some geotectonic hypotheses by paleomagnetism. Tectonophysics 1 (1), 3–71.
Van Houten, F., 1976. Late Variscan Nonmarine Basin Deposits, Northwest Africa: Record of Hercynotype Orogeny, the Continental Permain in Central, West, and South Europe. Springer, Amsterdam, pp. 215–224.
Visser, J.N., Praekelt, H.E., 1998. Late Palaeozoic crustal block rotations within the Gondwana sector of Pangea. Tectonophysics 287 (1–4), 201–212.
Voigt, S., Lagnaoui, A., Hminna, A., Saber, H., Schneider, J.W., 2011a. Revisional notes on the Permian tetrapod ichnofauna from the Tiddas Basin, Central Morocco. Palaeogeogr. Palaeoclimatol. Palaeoecol. 302 (3–4), 474–483.
Voigt, S., Saber, H., Schneider, J.W., Hmich, D., Hminna, A., 2011b. Late Carboniferous-early Permian Tetrapod Ichnofauna from the Khenifra Basin, Central Morocco. Geobios 44 (4), 399–407.
Wack, M.R., Gilder, S.A., 2012. The SushiBar: an automated system for paleomagnetic investigations. Geochem. Geophys. Geosyst. 13 (3).
Watson, G.S., Enkin, R.J., 1993. The fold test in paleomagnetism as a parameter estimation problem. Geophys. Res. Lett. 20 (19), 2135–2137.
Wernert, P., Schulmann, K., Chopin, F., Stipska, P., Bosch, D., El Houicha, M., 2016. Tectonometamorphic evolution of an intracontinental orogeny inferred from P-T-t-d paths of the metapelites from the Rehamna massif (Morocco). J. Metamorph. Geol. 34 (9), 917–940.
Wessel, P., Luis, J., Uieda, L., Scharroo, R., Wobbe, F., Smith, W.H., Tian, D., 2019. The generic mapping tools version 6. Geochem. Geophys. Geosyst. 20 (11), 5556–5564.
Westphal, M., Montigny, R., Thuizat, R., Bardon, C., Bossert, A., Hamzeh, R., Rolley, J., 1979. Paléomagnétisme et datation du volcanisme permien, triasique et crétacé du Maroc. Can. J. Earth Sci. 16 (11), 2150–2164.
Wu, L., Kravchinsky, V.A., Potter, D.K., 2015. PMTec: a new MATLAB toolbox for absolute plate motion reconstructions from paleomagnetism. Comput. Geosci. 82, 139–151.
Wu, L., Murphy, J.B., Quesada, C., Li, Z.-X., Waldron, J.W., Williams, S., Pisarevsky, S., Collins, W.J., 2021. The amalgamation of Pangea: Paleomagnetic and geological observations revisited. GSA Bull. 133 (3–4), 625–646.
Wu, L., Pisarevsky, S., Li, Z.-X., Murphy, J.B., Liu, Y., 2024. A new reconstruction of Phanerozoic Earth evolution: toward a big-data approach to global paleogeography. Tectonophysics 230198.
Youbi, N., 1998. Le volcanisme «post-collisionnel»: un magmatisme intraplaque relié à des panaches mantelliques. Etude volcanologique et géochimique. In: Exemples d "application dans le Néoprotérozoïque terminal (PIII) de l" Anti-Atlas et le Permien du Maroc, thèse d'État. université de Marrakech.
Youbi, N., Cabanis, B., Chalot-Prat, F., Cailleux, Y., 1995. Histoire volcano-tectonique du massif permien de Khénifra (Sud-Est du Maroc Central). Geodin. Acta 8 (3), 158–172.
Youbi, N., Gaggero, L., Assafar, H., Hadimi, I., Boumehdi, M., Bensalah, M.K., Linnemann, U., Gärtner, A., Mata, J., Doblas, M., 2018. U-Pb Zircon Geochronological and Petrologic Constraints on the Post-Collisional Variscan Volcanism of the Khenifra Basin (Western Meseta, Morocco). In: 2nd International Congress on Permian and Triassic Stratigraphic and Petrogenetic Implications, pp. 53–54.
Zijderveld, J.D.A., 1967. In: Collinson, D.W., Creer, K.M., Runcorn, S.K. (Eds.), A. C. Demagnetization of rocks: Analysis of results. Elsevier, Amsterdam, pp. 254–286.
Zouicha, A., Voigt, S., Saber, H., Marchetti, L., Hminna, A., El Attari, A., Ronchi, A., Schneider, J.W., 2021. First record of permian continental trace fossils in the jebilet massif, Morocco. J. Afr. Earth Sci. 173.
Zouicha, A., Saber, H., Attari, A.E., Zouheir, T., Ronchi, A., 2022. Late Hercynian tectonic evolution of the Jebilet Massif (Western Meseta, Morocco) based on tectono-sedimentary analyses of related Permian continental deposits. J. Iber. Geol. 1–27.
Zouine, E., 1986. Evolution structurale tardi-hercynienne de la bordure septentrionale du Maroc Central entre Tiddas et Jbel Triona. Unpublished Master Thesis. Ecole Nationale Supérieure du Souissi, Rabat.